HHS Public Access

Author manuscript

Nat Metab. Author manuscript; available in PMC 2025 January 21.

Published in final edited form as:

Nat Metab. 2022 November ; 4(11): 1474–1494. doi:10.1038/s42255-022-00664-z.

Adipose tissue macrophages exert systemic metabolic control by manipulating local iron concentrations

Nolwenn Joffin[1,5], **Christy M. Gliniak**[1,5], **Jan-Bernd Funcke**[1], **Vivian A. Paschoal**[1], **Clair Crewe**[1,2], **Shiuhwei Chen**[1], **Ruth Gordillo**[1], **Christine M. Kusminski**[1], **Da Young Oh**[1], **Werner J. Geldenhuys**[3], **Philipp E. Scherer**[1,4]

[1]Touchstone Diabetes Center, Department of Internal Medicine, University of Texas Southwestern Medical Center, Dallas, TX, USA.

[2]Department of Cell Biology, Washington University, St. Louis, MO, USA.

[3]Department of Pharmaceutical Sciences, West Virginia University, Morgantown, WV, USA.

[4]Department of Cell Biology, University of Texas Southwestern Medical Center, Dallas, TX, USA.

[5]These authors contributed equally: Nolwenn Joffin, Christy M. Gliniak.

Abstract

Iron is essential to many fundamental biological processes, but its cellular compartmentalization and concentration must be tightly controlled. Although iron overload can contribute to obesity-associated metabolic deterioration, the subcellular localization and accumulation of iron in adipose tissue macrophages is largely unknown. Here, we show that macrophage mitochondrial iron levels control systemic metabolism in male mice by altering adipocyte iron concentrations. Using various transgenic mouse models to manipulate the macrophage mitochondrial matrix iron content in an inducible fashion, we demonstrate that lowering macrophage mitochondrial matrix iron increases numbers of M2-like macrophages in adipose tissue, lowers iron levels in adipocytes, attenuates inflammation and protects from high-fat-diet-induced metabolic deterioration. Conversely, elevating macrophage mitochondrial matrix iron increases M1-like macrophages and iron levels in adipocytes, exacerbates inflammation and worsens high-fat-diet-induced metabolic dysfunction. These phenotypes are robustly reproduced by transplantation of a small amount of fat from transgenic to wild-type mice. Taken together, we identify macrophage mitochondrial iron levels as a crucial determinant of systemic metabolic homeostasis in mice.

Correspondence and requests for materials should be addressed to Philipp E. Scherer. philipp.scherer@utsouthwestern.edu.

Author contributions

Conceptualization, N.J., C.M.G, V.A.P., D.Y.O. and P.E.S.; methodology, N.J. and C.M.G; formal analysis, N.J., V.A.P. and C.C; investigation, N.J., C.M.G., J.-B.F., V.A.P., C.C., S.C., R.G. and C.M.K.; resources, W.J.G.; original draft writing, N.J. and P.E.S.; manuscript review and editing, N.J., C.M.G., J.-B.F. and P.E.S.; supervision, P.E.S.; funding acquisition, P.E.S.

Competing interests

The authors declare no competing interests.

Additional information

Extended data is available for this paper at https://doi.org/10.1038/s42255-022-00664-z.

Supplementary information The online version contains supplementary material available at https://doi.org/10.1038/s42255-022-00664-z.

White adipose tissue (WAT) fulfills diverse functions. Among these, it constitutes the main site of lipid storage in mammals with adipocytes taking up and releasing fatty acids in accordance with alterations in energy availability and demand. WAT function is crucial to maintain lipid homeostasis and protect other organs from lipotoxicity leading to insulin resistance[1–7].

Immune cells play an important supportive role in regulating adipocyte function in the WAT microenvironment. In both the lean and obese setting, WAT contains an almost full complement of innate and adaptive immune cells. However, their relative proportions change with obesity, contributing to sustained inflammation and insulin resistance[8]. The most abundant type of immune cells in WAT are adipose tissue macrophages (ATMs), which can constitute up to 50% of the stromal-vascular fraction (SVF) of WAT during obesity. The interplay between ATMs and adipocytes impacts the inflammatory state of adipose tissue and metabolism at large[9,10].

The link between obesity, inflammation and adipocyte iron overload is an area of emerging interest. Recent elegant studies have defined a subset of macrophages in WAT possessing a high iron content. These cells have been referred to as MFe^{hi} and exhibit a gene expression profile indicative of improved iron handling, a capacity that diminishes with obesity[11,12]. MFe^{hi} cells display an elevated expression of genes involved in iron uptake, such as *Cd163* and transferrin receptor-1 (*Tfrc*), iron metabolism, such as haem oxygenase-1 (*Hmox1*), iron storage, such as ferritin light and heavy chains (*Ftl1* and *Fth1*), as well as iron release, such as ferroportin (FPN, encoded by *Slc40a1*/*Fpn1*). In lean mice, MFe^{hi} cells represent ~25% of all ATMs and exhibit characteristics of alternatively activated M2-like macrophages[11,12]. However, the percentage of these cells decreases during obesity, leading to the recruitment of macrophages with a low-iron content referred to as MFe^{lo} cells and a shift of MFe^{hi} cells to a pro-inflammatory state. These changes in macrophages also result in a reduced local buffering capacity for iron, which causes adipocytes to experience iron overload.

Iron homeostasis plays an important role in adipocyte function with both adipogenesis and adipocyte lipid handling regulated by iron[13]). Adipocyte iron overload during obesity increases lipolysis and lipid peroxidation, leading to ectopic lipid deposition in other tissues[14,15]. Mitochondrial proteins, such as those forming the electron transport chain, are enriched in iron, rendering iron an important regulator of mitochondrial function. Excessively high iron levels in adipocytes undermine both mitochondrial function and adiponectin production, thereby contributing to the development of systemic insulin resistance[16,17]. This emphasizes the importance of a tight regulation of iron levels in WAT, which prompted us to assess the specific role that macrophages play in this process. In a parallel study, we addressed the impact of iron depletion from adipocytes through elimination of the transferrin receptor in these cells[14].

Cellular metabolism, especially mitochondrial metabolic pathways, plays a critical role in the maintenance of plasticity and making of fate decisions in various cell types, including macrophages[13,18,19]. Mitochondrial iron can thus also affect the polarization and function of macrophages[20–23]. However, a concise understanding of how mitochondrial iron shapes macrophage polarization and function is still lacking.

Here, we study the role of the mitochondrial iron balance in macrophages in the context of obesity. This is distinct from the other studies mentioned above that focused on total cytoplasmic iron in macrophages. We use three inducible transgenic mouse models to selectively manipulate the mitochondrial iron content in macrophages and demonstrate that such manipulations have pronounced effects not only on the function of these macrophages but also their local microenvironment and systemic metabolism. Our experiments reveal that depleting iron from the mitochondrial matrix of macrophages promotes cellular iron storage and an anti-inflammatory state. We determine that such a depletion also protects adipocytes from iron overload and preserves their function in the context of a high-fat diet (HFD) challenge, preventing and even reversing obesity and systemic metabolic dysfunction. We furthermore show that overloading the mitochondrial matrix of macrophages with iron in turn promotes cellular iron storage and a pro-inflammatory state. It furthermore exacerbates adipocyte iron overload, adipocyte dysfunction, obesity and systemic metabolic decline following HFD feeding. Overall, these observations highlight the substantial therapeutic potential of targeting macrophage mitochondrial iron content in the context of obesity and type 2 diabetes.

Results

Obesity leads to mitochondrial iron overload in adipose tissue macrophages

Our initial question was whether obesity promotes iron overload in adipocytes and macrophages. To address this question, we measured total iron levels (free and protein-bound iron) by inductively coupled plasma mass spectrometry (ICP-MS). Total iron levels were significantly increased in both adipocytes and peritoneal macrophages from HFD mice compared to chow mice (Fig. 1a). The effect of obesity was specific to iron, as obesity did not change copper levels (Fig. 1b). Next, we examined the labile iron pool (LIP; free iron) in ATMs purified from epididymal white adipose tissue (eWAT) of chow mice and HFD mice. In comparison to ATMs from chow mice, ATMs from HFD mice exhibited a decreased LIP (Fig. 1c). In contrast, adipocytes displayed an increased LIP in the HFD mice compared to chow mice (Fig. 1d). To better understand the regulation of iron in both cell types, we evaluated the expression of several regulators of cellular iron metabolism. The expression levels of iron uptake genes *Tfrc* and *Cd163* were decreased in HFD compared to chow ATMs, while those of *Lrp1* (*Cd91*), another iron uptake receptor, were increased. This suggests more iron uptake in the ATMs of HFD mice via CD91 (Fig. 1e). It is important to note that CD91 also serves as a marker of pro-inflammatory macrophages, while CD163 serves as a marker of anti-inflammatory macrophages[24]. Moreover, *Slc40a1* (*Fpn1*) expression was reduced on both the mRNA and protein levels, suggesting reduced iron release from obese macrophages (Fig. 1e,f,h). The expression levels of genes that promote iron storage, *Fth1* and *Ftl1*, in contrast, were increased (Fig. 1e). These results may explain the previous observation that, while total iron content is elevated, ATMs from mice with obesity display a reduced LIP[11]. This is likely due to the concomitant decrease in iron release by FPN. Further gene expression analyses in adipocytes from HFD mice revealed increases in *Cd91*, *Cd163*, *Slc11a2* (*Dmt1*), *Slc40a1* and *Ftl1* expression, suggesting a balance between iron uptake, storage and release (Fig. 1i). *Hmox1* mRNA expression increased in these cells (Fig. 1i). This aligns with previous studies establishing

HMOX1 as a marker of both iron overload and insulin resistance in adipocytes[25,26]. We also confirmed increased FTH1 expression and thus iron storage in adipocytes on the protein level (Fig. 1k,l). Furthermore, FPN expression decreased, suggesting reduced iron release from adipocytes (Fig. 1j,l). These results are supported by previous publications demonstrating that iron overload occurs in adipocytes during obesity[11,16].

Next, we examined how mitochondrial iron content is affected by obesity. For peritoneal macrophages, total cytoplasmic and mitochondrial iron levels were not different between the lean and obese states (Fig. 1m). Furthermore, we observed no difference in total mitochondrial content as judged by mitochondrial transcription factor A (encoded by *Tfam*) expression (Fig. 1n). However, MitoNEET (encoded by *Cisd1*) expression was lower, while mitochondrial ferritin (encoded by *Ftmt*) expression was higher in ATMs from HFD mice (Fig. 1n). MitoNEET protein expression was also decreased, whereas FTMT protein expression was increased (Fig. 1h,o,p). These results show that obesity favours mitochondrial matrix iron overload in macrophages by decreasing *Cisd1*, which can restrict mitochondrial matrix iron, and by increasing *Ftmt*, which can mediate mitochondrial matrix iron import and sequestration. In adipocytes, there were no differences on the mRNA level but MitoNEET protein expression decreased with obesity, consistent with increased matrix iron content (Fig. 1l,q,r). Furthermore, on the whole-tissue level, eWAT mitochondrial and cytosolic free iron levels were increased during obesity (Fig. 1s). Taken together, these results strongly support the view that mitochondria of ATMs and adipocytes display iron overload in the context of obesity.

MitoNEET overexpression in macrophages reduces mitochondrial iron

The notable differences in ATM mitochondrial iron metabolism between the lean and obese states raise the question of how this disruption of iron homeostasis affects the functional properties of ATMs. To address this, we established inducible transgenic mouse models in which the mitochondrial iron content of macrophages can be regulated in a doxycycline (dox)-dependent manner through the expression of either MitoNEET (leading to a decrease in mitochondrial iron content) or FTMT (leading to an increase in mitochondrial iron content). MitoNEET is an iron-containing outer mitochondrial membrane protein that reduces the iron content of mitochondria and reduces mitochondrial activity[27,28]. FTMT displays ferroxidase activity, promoting chelation and storage of iron within the mitochondrial matrix similar to ferritin in the cytosol[29,30]. Our bi-transgenic ‘Tet-On’ models consist of the previously described *Csf1r*-rtTA allele in combination with either the *TRE*-MitoNEET or the *TRE*-Ftmt allele (herein, Mac-MitoNEET^{TG} or Mac-Ftmt^{TG} mice)[13,30,31] (Extended Data Figs. 1a and 2a). First, we aimed to validate our mouse models by feeding control and overexpressing animals with a chow diet containing dox (chow dox) and isolating monocytes and ATMs from eWAT as well as peritoneal macrophages. As expected, we observed an increased *Cisd1* (MitoNEET) expression in monocytes, ATMs and peritoneal macrophages in Mac-MitoNEET^{TG} mice and an increased *Ftmt* expression in ATMs of Mac-Ftmt^{TG} mice (Extended Data Figs. 1b and 2b). MitoNEET and FTMT protein expression was doubled compared to controls (Extended Data Figs. 1c,d and 2c,d). MitoNEET and FTMT overexpression both lead to a decrease in mitochondrial oxidative metabolism in multiple cell types[13,27,28,30]. We isolated peritoneal macrophages

from control, Mac-MitoNEET^{TG} and Mac-Ftmt^{TG} mice fed chow dox for 2 weeks and evaluated their oxidative and glycolytic metabolic activity. In macrophages from both Mac-MitoNEET^{TG} and in Mac-Ftmt^{TG} mice, oxidative metabolism was reduced (Extended Data Figs. 1e,f and 2e,f). This reduction in oxidative metabolism was due to a decrease in mitochondrial complex expression, especially complexes enriched in iron–sulfur (Fe–S) clusters such as complex I, II and III in the MitoNEET^{TG} group (Extended Data Fig. 1g,h). Surprisingly, complex IV and V expression increased in MitoNEET^{TG} mice, suggesting compensation occurred (Extended Data Fig. 1g,h). In Mac-Ftmt^{TG} mice, only complex V expression decreased (Extended Data Fig. 2g,h). For both models, the decrease in oxidative metabolism did not coincide with any increase in glycolytic metabolism (Extended Data Figs. 1i,j and 2i,j). One limitation of our interpretation of the mitochondrial respiration data as it applies to ATMs, is that peritoneal macrophages were used due to technical constraints. The adipose tissue niche may contribute to differences in iron dynamics that regulate mitochondrial respiration in macrophages that are lost in peritoneal macrophages. Yet, we do observe a fundamental role of MitoNEET or FTMT expression on respiration in the peritoneal macrophages, as the proteins were inducibly and directly overexpressed in the cells. Furthermore, these data are in line with our previous studies[13,27,28,30], suggesting that, independent of the affected cell type, a delicate regulation of mitochondrial iron levels is essential for proper mitochondrial function.

We subsequently assessed the LIP and its dynamics in both transgenic models on chow dox. In Mac-MitoNEET^{TG} mice, peritoneal macrophages exhibited a lower LIP in the mitochondrial fraction, and no change in the cytosolic LIP was observed (Extended Data Fig. 3a). Overexpression of MitoNEET in macrophages led to a decrease in the mRNA expression of *Cd91*, a receptor for haemopexin-bound haem iron and marker of inflammatory macrophages (Extended Data Fig. 3b). There were no changes on the protein level for FTH1, FPN, CD163, CD91 or FTMT (Extended Data Fig. 3c–h). For peritoneal macrophages from Mac-Ftmt^{TG} mice, the mitochondrial LIP increased compared to controls, while again, no change in cytosolic LIP was observed (Extended Data Fig. 4a). Iron uptake pathways were upregulated, as *Cd91* mRNA and protein levels were increased, while *Cd163* mRNA and protein expression was unaltered (Extended Data Fig. 4b–d,h). Iron storage was enhanced, as *Hmox1*, *Fth1* and *Ftl1* mRNA expression were increased (Extended Data Fig. 4b,e,d,h). While *Slc40a1* mRNA was decreased, its protein level remained unchanged (Extended Data Fig. 4f,h). Moreover, while *Fth1* mRNA was increased, its protein level was decreased, suggesting a diminished iron storage capacity (Extended Data Fig. 4e–h). In line with the increase in mitochondrial iron content, MitoNEET protein decreased in peritoneal macrophages from Mac-Ftmt^{TG} mice, supporting further iron retention in the mitochondrial matrix (Extended Data Fig. 4g,h). Altogether, these results suggest that overexpressing MitoNEET in macrophages prevents mitochondrial iron overload by promoting gene expression that supports increased release of cytosolic iron. In contrast, overexpressing FTMT in macrophages favours iron uptake and retention in the mitochondria. Thus, these two mouse models exhibit opposite changes in mitochondrial free iron content.

Macrophage mitochondrial iron alters inflammatory properties

We next aimed to understand the impact of mitochondrial iron overload on macrophage function. After 2 weeks of chow dox feeding, gene expression analyses of inflammatory markers revealed that mitochondrial iron depletion led to an anti-inflammatory phenotype, while mitochondrial iron overload led to a pro-inflammatory phenotype. Peritoneal macrophages from Mac-MitoNEET^{TG} mice exhibited lower pro-inflammatory *Cd11c* and *Il6* as well as higher anti-inflammatory *Il13* expression (Extended Data Fig. 3i). In eWAT from these mice, the number of total macrophages and proportion of M1-like macrophages were decreased, while the proportion of M2-like macrophages remained unchanged (Extended Data Fig. 3j–l). In peritoneal macrophages from Mac-Ftmt^{TG} mice, the expression of pro-inflammatory *Cd11c, Ccl2*, *Il1b* and *Tnfa* increased and the expression of anti-inflammatory *Il10* decreased (Extended Data Fig. 4i). There were no changes in the number of total macrophages or proportion of M1-like and M2-like macrophages (Extended Data Fig. 4j–l). Altogether, these results demonstrate that manipulating mitochondrial matrix iron from low to high levels leads to divergent macrophage phenotypes. While mitochondrial iron depletion promotes anti-inflammatory properties, mitochondrial iron overload promotes pro-inflammatory ones.

On a chow dox diet, Mac-MitoNEET^{TG} and control mice did not display any differences in body weight, glucose tolerance, insulin sensitivity or triglyceride clearance (Extended Data Fig. 3m–q). Similarly, on the same chow dox diet, Mac-Ftmt^{TG} mice exhibited no changes in body weight, glucose tolerance, insulin sensitivity and triglyceride clearance but glucose-stimulated insulin release was reduced (Extended Data Fig. 4m–q). These results highlight that, under chow diet conditions, manipulating mitochondrial matrix iron content in macrophages affects their inflammatory properties and metabolic functions, but does not have a profound effect on either body weight or systemic metabolism.

Macrophage mitochondrial iron affects adipocyte iron metabolism

Diet-induced obesity is associated with local inflammation and iron overload in adipose tissue, resulting in detrimental consequences for the whole body. We demonstrated that obesity is accompanied by a decrease in MitoNEET and increase in FTMT expression in macrophages, partially explaining the mitochondrial iron overload observed in these cells. The anti-inflammatory and pro-inflammatory phenotypes observed in Mac-MitoNEET^{TG} and Mac-Ftmt^{TG} macrophages, respectively, prompted us to assess the manipulation of mitochondrial matrix iron in the context of obesity. Mac-MitoNEET^{TG} and Mac-Ftmt^{TG} mice were fed a HFD containing dox (HFD dox) for 6 weeks. We then isolated ATMs and adipocytes from eWAT and assessed their iron content. As previously shown on chow dox, macrophage mitochondrial iron depletion by MitoNEET overexpression during HFD dox led to a decrease in the LIP in ATMs (Extended Data Fig. 5a); however, no change in total iron was observed in the mitochondrial or cytosolic fraction of macrophages (Extended Data Fig. 5b). Interestingly, adipocytes displayed a reduced LIP, while no changes were apparent in the remainder of the SVF (Extended Data Fig. 5c,d). In adipocytes from Mac-MitoNEET^{TG} eWAT, *Hmox1* mRNA decreased, in line with the lower LIP in these cells (Extended Data Fig. 5e). In agreement with our previous data from mice fed chow dox, *Cd163*, *Slc40a1* and *Fth1* expression increased, while *Ftl1* expression decreased in ATMs, suggesting an overall

increase in iron cycling (uptake, storage and release; Extended Data Fig. 5f). In adipocytes from Mac-MitoNEET^{TG} animals, *Slc40a1* and *Fth1* mRNA levels decreased, while their protein levels increased (Extended Data Fig. 5e,g–i). This increase in iron release is in line with the decrease of the LIP in adipocytes (Extended Data Fig. 5c). In ATMs, CD91 was not changed, but iron uptake and storage were increased by an upregulation of CD163 and FTH1 (Extended Data Fig. 5j,k,m,n). FPN protein levels were increased, arguing for a change in the regulation of proteins associated with iron cycling in ATMs (Extended Data Fig. 5l,n). As expected, *Cisd1* mRNA and MitoNEET protein were upregulated in ATMs from Mac-MitoNEET^{TG} animals, while *Ftmt* mRNA and protein expression remained unchanged (Extended Data Fig. 5n–q). We also observed that iron translocation into the mitochondria of adipocytes may be limited, as there was an increase in MitoNEET protein (Extended Data Fig. 5i,r). Furthermore, the mitochondrial LIP in eWAT decreased, while the cytosolic LIP was unchanged (Extended Data Fig. 5s). In agreement with our previous observations under chow dox conditions, depleting iron from the mitochondria in macrophages led to a decrease of the M1-like macrophage marker *Cd11c* and the pro-inflammatory cytokine *Il6* (Extended Data Fig. 5t). In contrast, anti-inflammatory cytokines *Il4*, *Il10* and *Il13* were increased (Extended Data Fig. 5t). In adipocytes of Mac-MitoNEET^{TG} mice, pro-inflammatory cytokines such as *Tnfa* and *Il1b* decreased (Extended Data Fig. 5u). Moreover, eWAT from Mac-MitoNEET^{TG} produced less reactive oxygen species (ROS) as indicated by a decrease in lipid peroxidation and protein carbonylation (Extended Data Fig. 5v–x). These results demonstrate that protecting ATMs from mitochondrial iron overload during obesity has a profound impact on WAT, especially adipocyte iron content, affecting the overall inflammatory profile of the tissue, protecting it from oxidative damage, and preserving its metabolic functions.

Mac-Ftmt^{TG} mice fed HFD dox displayed an opposite phenotype to Mac-MitoNEET^{TG} mice. Peritoneal macrophages from Mac-Ftmt^{TG} exhibited a decrease in their cytosolic total iron content and a 27.6% increase in mitochondrial total iron content at a p-value of 0.0009 (Extended Data Fig. 6a). Overloading ATM mitochondria with iron also increased the ATM and adipocyte LIP and decreased the SVF LIP (Extended Data Fig. 6b–d). Adipocytes expressed elevated levels of iron uptake genes such as *Tfrc* and *Hmox1*, consistent with an increase in iron uptake and content (Extended Data Fig. 6e). A decrease in FPN protein expression indicated a compromised release of iron from adipocytes, whereas FTH1 protein expression was unchanged, hinting at unaltered iron storage (Extended Data Fig. 6g–i). In ATMs, iron uptake was increased as judged by an increase in *Cd91* (Extended Data Fig. 6f). This increase in iron uptake was not compensated for by any increase in iron storage, as FTH1 protein expression was unchanged in ATMs of Mac-Ftmt^{TG} mice (Extended Data Fig. 6j,l). This iron overload was exacerbated by a decrease in iron release, as indicated by a reduction in FPN (Extended Data Fig. 6k–l). As previously shown, *Ftmt* expression was significantly increased in ATMs from Mac-Ftmt^{TG} mice, while *Cisd1* expression was not changed (Extended Data Fig. 6m). In contrast, adipocytes from Mac-Ftmt^{TG} mice displayed a decrease in MitoNEET protein expression, contrasting our observations in Mac-MitoNEET^{TG} mice (Extended Data Fig. 6i,n). The mitochondrial iron overload in ATMs was accompanied by an increase in the mitochondrial LIP in whole eWAT of Mac-Ftmt^{TG} mice (Extended Data Fig. 6o). Mac-Ftmt^{TG} mice displayed a pro-inflammatory

ATM phenotype with an upregulation of the pan-macrophage markers *F4/80* and *Cd11b* and an increase in the M1-like macrophage marker *Cd11c* (Extended Data Fig. 6p). This was accompanied by higher levels of the pro-inflammatory cytokines *Ccl2*, *Il1b* and *Il6* and lower levels of the anti-inflammatory cytokines *Il4* and *Il10* (Extended Data Fig. 6p). In adipocytes, the expression of pro-inflammatory markers *Il1b*, *Ccl2* and *Tlr4* increased (Extended Data Fig. 6q). Altogether, we conclude that mitochondrial iron overload in macrophages during obesity promotes local inflammation and iron overload in cells beyond the macrophage.

Macrophage mitochondrial iron depletion promotes metabolic health

Based on our HFD dox experiments, we hypothesized that Mac-MitoNEET^{TG} mice would be protected from inflammation and adipocyte dysfunction. To explore this further, we fed Mac-MitoNEET^{TG} mice HFD dox for up to 20 weeks. The body weight gain was reduced in the transgenic mice (Fig. 2a). After 6 weeks of HFD dox feeding, Mac-MitoNEET^{TG} mice had lower adipose tissue mass, particularly subcutaneous white adipose tissue (sWAT) and eWAT mass (Fig. 2b). Strikingly, serum adiponectin levels remained unchanged (Fig. 2c), and fasting serum insulin levels were reduced in Mac-MitoNEET^{TG} mice (Fig. 2d). Adipose tissue histology revealed pronounced differences between Mac-MitoNEET^{TG} and control sWAT, eWAT and retroperitoneal white adipose tissue with overall smaller adipocytes in transgenic mice (Fig. 2e). Furthermore, the livers of Mac-MitoNEET^{TG} mice contained fewer lipid droplets and their pancreatic islets were smaller (Fig. 2e). The glucose tolerance and insulin sensitivity of Mac-MitoNEET^{TG} mice also improved (Fig. 2f–h). These effects persisted even after 20 weeks of HFD dox feeding (Fig. 2i–l).

In eWAT, ROS production decreased in MitoNEET^{TG} mice, as judged by a reduction in 4-hydroxynonenal (4-HNE) levels (Fig. 2m,n). Moreover, the total number of macrophages decreased in both sWAT and eWAT (Fig. 2o). This decrease was due to a reduction in M1-like macrophage frequency in eWAT, while anti-inflammatory M2-like macrophages were more abundant (Fig. 2p,q). In sWAT, the frequency of M1-like macrophages did not change, but the M2-like population increased significantly (Fig. 2p,q). These results demonstrate that there are metabolic benefits during obesity by protecting ATMs from mitochondrial iron overload, which also translates to reduced adipocyte iron levels.

We also explored the body weight and metabolic homeostasis of Mac-Ftmt^{TG} mice fed HFD dox for up to 20 weeks. In contrast to Mac-MitoNEET^{TG} mice, Mac-Ftmt^{TG} mice gained more weight than their controls (Fig. 3a). The increase in body weight was due to increases in sWAT, eWAT and liver mass (Fig. 3b). Serum adiponectin levels were unchanged compared to control mice, despite increased fat mass (Fig. 3c). However, serum insulin levels in both the fed and fasted states were increased in the Mac-Ftmt^{TG} mice, suggesting insulin resistance (Fig. 3d). Histology revealed exacerbated sWAT and eWAT inflammation concomitant with increased liver steatosis in Mac-Ftmt^{TG} mice (Fig. 3e). As expected, insulin resistance was impaired as early as 6 weeks of HFD dox feeding (Fig. 3f–h). As observed in Mac-MitoNEET^{TG} mice, these effects persisted, even after 20 weeks of HFD dox feeding (Fig. 3i–k). Mitochondrial iron overload in ATMs led to an increase in M1-like macrophages, while total macrophages remained unchanged in both sWAT and

eWAT (Fig. 3l,m). Mac-Ftmt^{TG} mice displayed reduced M2-like macrophages in sWAT (Fig. 3n).

To further characterize how mitochondrial iron overload in macrophages exacerbates the systemic response to HFD, we generated a mouse model with an inducible, macrophage-specific loss of MitoNEET (Mac-MitoNEET^{KO}; Extended Data Fig. 7a–c). After 7 weeks of HFD dox feeding, body weight did not differ between Mac-MitoNEET^{KO} and control mice (Extended Data Fig. 7d). However, Mac-MitoNEET^{KO} mice displayed enlarged livers and increased sWAT mass (Extended Data Fig. 7e). In contrast to the overexpression of MitoNEET in macrophages, glucose tolerance and insulin sensitivity were worsened in Mac-MitoNEET^{KO} mice (Extended Data Fig. 7f–h). Of note, at 7 weeks of HFD dox feeding, we observed no changes in total macrophage numbers or the proportions of M1-like and M2-like macrophages in eWAT of these mice (Extended Data Fig. 7i–k). These findings demonstrate that macrophages are sensitive to a loss as well as gain in mitochondrial iron levels during obesity and that these changes result in opposite systemic metabolic phenotypes in the context of obesity. Altogether, these results from multiple mouse models highlight the crucial role mitochondrial iron homeostasis in ATMs plays in maintaining adipocyte function, adipose tissue health, and thus also systemic metabolism.

Macrophage mitochondrial iron depletion reverses effects of high-fat diet

Mitochondrial iron depletion in ATMs has been shown to be metabolically beneficial during obesity development. Therefore, we wondered whether protecting mitochondria from iron overload after obesity had already been established could reverse some of the detrimental consequences. To address this question, we fed Mac-MitoNEET^{TG} mice a HFD for 20 weeks. At that point, we induced MitoNEET overexpression by switching to HFD dox (Fig. 4a). Mitochondrial iron depletion in ATMs drastically reduced body weight within just a few days following the switch from HFD to HFD dox (Fig. 4b). After 6 weeks of HFD dox, the total body fat of Mac-MitoNEET^{TG} mice was substantially reduced, while their lean mass was higher compared to control mice (Fig. 4c). sWAT and brown adipose tissue (BAT) mass reduced in the transgenic group, while eWAT mass was unchanged (Fig. 4d). Triglyceride clearance improved in Mac-MitoNEET^{TG} mice compared to control animals, suggesting an enhanced ability of adipose tissue to store lipids, which is consistent with the fact that Mac-MitoNEET^{TG} mice are more insulin sensitive (Fig. 4e). On the histological level, sWAT and eWAT contained fewer crown-like structures, indicative of attenuated inflammation and in line with our previous observations under chow dox or continuous HFD dox conditions (Fig. 4f). The livers of Mac-MitoNEET^{TG} mice contained less lipids compared to the controls (Fig. 4f), reflecting the improvements in adipose tissue. Adiponectin and leptin mRNA expression increased specifically in eWAT and the serum levels of both adipokines were elevated (Fig. 4g–j). We measured iron in the serum of these mice as early at 2 d after switching to HFD dox as well as at 10 d, 12 d and 6 weeks after. While serum iron levels did not differ 2 d after the diet change, an increase was seen at 10 d, followed by a net decrease after 6 weeks of HFD dox feeding (Fig. 4k).

As previously described for continuous HFD dox feeding, switching mice to HFD dox after long-term HFD feeding resulted in metabolic benefits for Mac-MitoNEET^{TG} mice. These

mice were more glucose tolerant and insulin sensitive (Fig. 4l–n). As previously shown on chow dox and HFD dox, sWAT and eWAT of Mac-MitoNEET^{TG} mice were less inflamed, expressing lower levels of the pan-macrophage markers *F4/80* and *Cd11b*, the M1-like macrophage marker *Cd11c*, and the pro-inflammatory cytokines *Tnfa*, *Il6* and *Il1b*, as well as higher levels of the anti-inflammatory cytokine *Il13* (Fig. 4o,p). Both adipose depots in Mac-MitoNEET^{TG} mice contained a decreased proportion of total macrophages and increased proportion of M2-like macrophages (Fig. 4q–s). This decrease in inflammation was accompanied by an increase in antioxidant gene expression in eWAT, while the mitochondrial marker *Tfam* was unchanged between groups (Fig. 4t–w). In line with our previous data on HFD dox, these results suggest lower production of ROS contributed to an improved, more functional adipose tissue. To understand how the mice lose weight so rapidly, we repeated the experiment after the mice acclimatized to the HFD, and then afterwards, mice were fed HFD dox for 7 d to simultaneously measure parameters of energy intake and expenditure in metabolic cages (Extended Data Fig. 8a). Body weights of both control and transgenic animals were not different before switching to HFD dox (Extended Data Fig. 8b). The parameters measured in the metabolic cages during the 3 d before switching the diet were not different either (Supplementary Table 1). Remarkably, after just 3 d of HFD dox feeding, Mac-MitoNEET^{TG} animals lost weight (Extended Data Fig. 8b and Supplementary Table 2). This reduction of body weight was associated with a decrease in the respiratory exchange ratio (Extended Data Fig. 8d), suggesting the preferred use of lipids over carbohydrates as the energetic substrate. Food intake, energy balance, and the difference between calorie intake and expenditure, were lower in these mice (Extended Data Fig. 8c,e and Supplementary Table 2). Altogether, our experiments demonstrate a robust beneficial effect of depleting mitochondrial iron in ATMs. This can protect and even rescue mice from the deleterious metabolic consequences of diet-induced obesity.

Mac-MitoNEET^{TG} and Mac-Ftmt^{TG} exert effects through adipose tissue

Because macrophages are found in variety of tissues, one of the central questions was which macrophage populations are the main contributors to the beneficial effects of MitoNEET as well as the detrimental effects of FTMT overexpression. To answer this question, we transplanted eWAT from control, Mac-MitoNEET^{TG} or Mac-Ftmt^{TG} mice orthotopically into wild-type mice. To validate our transplantation model, we injected the donor mice with the cell tracer PKH67 before eWAT transplantation. PKH67 is readily taken up by phagocytic cells and can be used to mark tissue-resident macrophages. Any PKH67^{+} cells detected at the end of the experiment must have been present at the time of PKH67 injection. In contrast, PKH67^{-} cells represent macrophages that were deposited later. Following transplantation, mice were allowed to recover for 3 weeks and were then fed HFD dox for 6 weeks (Fig. 5a). We harvested the graft and recipient eWAT and assessed PKH67 fluorescence by flow cytometry. After 6 weeks of HFD dox feeding, PKH67^{+} macrophages in eWAT represented around 30% of total macrophages in the graft (Extended Data Fig. 9a). This result highlights that macrophages from the donor were still present in the graft, reflecting a fully functional graft capable of maintaining its original cells. Furthermore, the presence of PKH67^{-} macrophages indicated the recruitment of monocyte-derived macrophages subsequent to PKH67 labelling, suggesting that the graft communicated with the recipient tissues to recruit cells (Extended Data Fig. 9a). Interestingly, around 7% of total

macrophages in the recipient eWAT were PKH67^{+}, arguing for a mutual exchange of cells between graft and recipient tissues (Extended Data Fig. 9b). Importantly, ATMs from the graft from Mac-MitoNEET^{TG} mice still overexpressed *Cisd1* (Extended Data Fig. 9c), while no increased *Cisd1* expression was detected in ATMs from the recipient eWAT (Extended Data Fig. 9d). We made similar observations for the overexpression of *Ftmt* in grafts from Mac-Ftmt^{TG} mice (Extended Data Fig. 9h,i). Following HFD dox feeding, the body weights of mice grafted with control, Mac-MitoNEET^{TG} and Mac-Ftmt^{TG} eWAT were comparable (Figs. 5b and 6b). Weight gain and food intake were comparable as well (Figs. 5c,d and 6c,d). Despite the lack of changes in these parameters, mice transplanted with eWAT from Mac-MitoNEET^{TG} mice were protected from glucose intolerance and insulin resistance as early as 2 weeks after the onset of HFD dox feeding (Fig. 5e–g). These beneficial effects were maintained after 6 weeks (Fig. 5i–k). Transplantation of Mac-Ftmt^{TG} eWAT, in contrast, had deleterious effects on glucose and insulin homeostasis at both 2 weeks and 6 weeks after initiation of HFD dox feeding (Fig. 6e–g,i–k). Triglyceride clearance improved in mice transplanted with Mac-MitoNEET^{TG} eWAT (Fig. 5h,l) and was disrupted in the mice transplanted with Mac-Ftmt^{TG} eWAT (Fig. 6h,l), suggesting changes in the efficacy of lipid disposal. sWAT, eWAT and liver weights were unchanged between groups (Figs. 5m and 6m)

As previously described for the Mac-MitoNEET^{TG} model, wild-type mice grafted with Mac-MitoNEET^{TG} eWAT also displayed lower iron content in ATMs, adipocytes and SVF cells from the graft eWAT (Fig. 5n–p). However, while ATMs from the recipient eWAT exhibited no changes in iron metabolism gene expression, they showed a higher expression of the anti-inflammatory marker *Cd206* (Fig. 5q,r). These results were further supported by flow cytometric analyses revealing an increase in the proportion of M2-like macrophages, while total and M1-like macrophages were unchanged in the recipient eWAT (Extended Data Fig. 9e–g). In line with our previous data on HFD dox feeding, the eWAT graft actively maintained enhanced iron metabolism with increases in *Cd163*, *Scl40a1*, *Fth1* and *Ftl1* and a decrease in *Hmox1* expression, consistent with reduced iron content (Fig. 5s). The eWAT graft also expressed lower levels of pro-inflammatory macrophage and cytokine markers *F4/80*, *Cd11b*, *Cd11c*, *Tnfa*, *Il1b* and *Il6*, along with higher levels of anti-inflammatory markers *Cd206*, *Il4* and *Il13* (Fig. 5t). Interestingly, the transplantation of Mac-MitoNEET^{TG} eWAT induced FPN protein expression in recipient eWAT adipocytes (Fig. 5u,x). However, no changes were observed in recipient eWAT with respect to FTH1 or MitoNEET protein expression (Fig. 5v–x). This indicated improved adipocyte function, a notion supported by increased serum adiponectin levels (Fig. 5y).

In contrast, mice transplanted with Mac-Ftmt^{TG} eWAT displayed a high iron content in ATMs and adipocytes, but not SVF cells from grafted eWAT (Fig. 6n–p). However, while ATMs from recipient eWAT did not exhibit any changes in iron metabolism gene expression, they were nonetheless affected by the graft inducing increased expression of the pro-inflammatory macrophage marker *Cd11c* and decreased expression of the anti-inflammatory macrophage marker *Cd206* (Fig. 6r). Grafts from Mac-Ftmt^{TG} mice retained a similar iron metabolism profile as that previously described in the Mac-Ftmt^{TG} model, exhibiting increased levels of iron uptake genes *Trf* and *Cd91* and decreased levels of the iron release gene *Slc40a1*, contributing to an overall higher iron content suggested

by an increased *Hmox1* level (Fig. 6s). The graft also retained a more pro-inflammatory expression pattern as indicated by increases in *F4/80*, *Cd11b*, *Cd11c*, *Ccl2*, *Tnfa* and *Il6* and a decrease in *Il13* expression (Fig. 6t). Regarding adipocytes, we observed no changes in the expression of iron metabolism proteins (Fig. 6u–x), but serum adiponectin levels were decreased (Fig. 6y). These results are all in accordance with what we observed in the adipose tissue of Mac-MitoNEET^{TG} and Mac-Ftmt^{TG} mice before transplantation.

Altogether, these results emphasize the powerful benefits gained from protecting macrophages from mitochondrial iron overload. As a reflection of the immense potency of the effects of these fat grafts, as little as 1% of total fat in the form of a transplant was able to alter the systemic metabolism over such an extended period. Hence, we attribute the effects we observed in these and previous experiments predominantly to fat-pad-autonomous factors that act in a paracrine and/or endocrine fashion.

Cross-talk between adipose tissue macrophages and adipocytes

To follow up the paracrine nature of these interactions, we went on to assess whether the observed effects are the reflection of a direct cross-talk between ATMs and adipocytes. We hypothesized that Mac-MitoNEET^{TG} ATM secretion products have immediate effects on adipocytes that preserve their function. We thus treated in vitro differentiated wild-type adipocytes with conditioned medium from either Mac-MitoNEET^{TG} or Mac-Ftmt^{TG} ATMs for 24 h, in the presence or absence of additional iron in the form of ferric ammonium citrate (FAC; Figs. 7a and 8a). Of note, to control for the presence of citrate during FAC treatment, cells were also treated with citrate alone. Citrate treatment did not alter the expression of iron-sensitive or adipocyte-specific genes in these experiments (Fig. 7b–d,j,l). In the presence of iron, adipocytes increased the expression of the iron export gene *Slc40a1*, possibly as a protective mechanism against overload (Figs. 7b and 8b). Strikingly, adipocytes treated with iron combined with conditioned medium from control macrophages failed to mount this protective response and displayed decreased *Slc40a1* levels (Figs. 7b and 8b). Interestingly, Mac-MitoNEET^{TG} ATM-conditioned medium evoked an increase in adipocyte *Slc40a1* expression. This increase was observed even without iron treatment, but further enhanced when additional iron was added to the conditioned media (Fig. 7b). These results support our previous in vivo observations of an increased expression of genes that regulate iron release from adipocytes of eWAT in Mac-MitoNEET^{TG} mice. Iron treatment of adipocytes also resulted in iron overload, as indicated by an increased expression of *Hmox1* (Fig. 7c). However, *Hmox1* levels were reduced when the iron treatment occurred in presence of Mac-MitoNEET^{TG} ATM-conditioned medium, reflecting a protection from iron overload (Fig. 7c). Mitochondrial iron content was more sensitive to iron overload when adipocytes were treated with control ATM-conditioned medium, as seen by decreased *Cisd1* expression (Fig. 7d). In contrast, treatment with Mac-MitoNEET^{TG} ATM-conditioned medium protected adipocytes from mitochondrial iron overload by upregulating *Cisd1* (Fig. 7d). On the protein level, treatment with iron increased FPN (Fig. 7e,h). While treatment of adipocytes with control ATM-conditioned medium decreased the capacity of adipocytes to release iron by decreasing FPN expression, Mac-MitoNEET^{TG} ATM-conditioned medium upregulated FPN expression (Fig. 7e,h); however, adipocyte FTH1 or MitoNEET protein levels did not change (Fig. 7f–h). To confirm that Mac-MitoNEET^{TG} ATM-conditioned

medium can protect adipocytes from iron overload, we measured the LIP, and iron treatment indeed led to a massive increase in adipocyte LIP (Fig. 7i). Interestingly, while control ATM-conditioned medium exacerbated iron overload in adipocytes, Mac-MitoNEET^{TG} ATM-conditioned medium was able to prevent this phenomenon (Fig. 7i). Adipocyte iron overload led to a decrease in adiponectin expression and secretion (Fig. 7j,k). As expected, the protection from iron overload when adipocytes were treated with Mac-MitoNEET^{TG} ATM-conditioned medium also alleviated these effects on adiponectin production (Fig. 7j,k). Importantly, these effects on adipocytes were also observed in the absence of iron overload, suggesting that Mac-MitoNEET^{TG} ATMs can promote adipocyte function independent of their effects on adipocyte iron levels (Fig. 7k). In accordance, we observed that Mac-MitoNEET^{TG} ATM-conditioned medium alone was able to maintain leptin levels comparable to non-treated adipocytes, while control ATM-conditioned medium decreased leptin levels (Fig. 7l). Mac-MitoNEET^{TG} ATM-conditioned medium increased both basal and maximal mitochondrial respiration independent of the presence of iron (Fig. 7m–o). These results suggest that adipocytes can be protected from the deleterious effects of iron overload when treated with Mac-MitoNEET^{TG} ATM-conditioned medium. In addition, some of the benefits of this treatment are independent of iron regulation. With these experiments, we demonstrate direct beneficial effects of Mac-MitoNEET ^{TG} ATM secretion products on adipocytes.

Mac-Ftmt^{TG} ATM-conditioned medium, in contrast, had deleterious effects on adipocytes. While it did not affect *Slc40a1* (Fig. 8b), and neither *Hmox1* nor *Cisd1* levels (Fig. 8c,d), it diminished iron release from adipocytes by decreasing FPN protein level (Fig. 8e,h). Mac-Ftmt^{TG} ATM-conditioned medium also increased the iron content in adipocytes after addition of iron to the treatment (Fig. 8i); however, at the protein level, FTH1 and MitoNEET were unchanged (Fig. 8e–h). Furthermore, it decreased adiponectin production, independent of the inclusion of additional iron (Fig. 8j,k). Moreover, it compromised adipocyte mitochondrial metabolism, both basal and maximal activity, independent of iron addition (Fig. 8m–o).

Altogether, these data argue for a direct effect from ATM secretion products on adipocytes. While the secretome of Mac-MitoNEET^{TG} ATMs protects adipocytes from the harmful effects of iron overload, the secretome of Mac-Ftmt^{TG} ATMs exacerbates this deleterious process. Importantly, some of the effects of these in vitro conditioned media experiments observed here are independent of iron overload, suggesting that Mac-MitoNEET^{TG} and Mac-Ftmt^{TG} ATMs communicate with adipocytes in complex ways.

Discussion

Macrophage mitochondrial iron content determines cell function

Iron is essential to many fundamental biological processes and must be carefully regulated. Excess iron can cause cellular and tissue damage if not controlled and properly sequestered, and is a risk factor associated with type 2 diabetes and other diseases[16,32–35]. In the obese state, iron overload contributes directly to the pro-inflammatory polarization of macrophages[36,37]. Tied to this, the polarization state of macrophages affects their iron metabolism. M1-like macrophages take up and sequester iron as a bacteriostatic mechanism,

while M2-like macrophages take up and release iron. This dogma has recently been challenged by the Hasty laboratory publishing a series of studies defining a population of alternatively activated ATMs termed MFe^{hi}, which are M2-polarized cells, exhibiting an iron cycling phenotype, a capacity that diminishes with obesity[11,12,38]. Here, we show that mitochondrial iron compartmentalization is essential to the regulation of macrophage polarization and function. Our study demonstrates how obesity dysregulates the mitochondrial uptake and release of iron in macrophages, partially through changes in MitoNEET and FTMT expression, and further delineates the tight link that exists between changes in compartmental iron levels and the dysregulation of macrophage and adipocyte function.

It is well established that obesity is linked to mitochondrial dysfunction[39]. Here, we examine the role that mitochondrial iron overload plays in the impairment of macrophage function during obesity. Studies involving acute experimental changes in mitochondrial iron metabolism during inflammation have hitherto been missing. In this study, we used three unique transgenic mouse models in which macrophage mitochondrial iron levels can be increased or decreased in a tightly controlled fashion. We show that MitoNEET overexpression in macrophages protects these cells from mitochondrial iron overload without affecting cytosolic iron content when on a chow dox diet. In a situation of iron overload, as seen during HFD feeding, macrophages overexpressing MitoNEET display an elevation in all iron metabolism-related genes and proteins quantified, including *Cd163*, *Fpn1* and *Fth1*, which was previously dubbed an ‘iron recycling’ phenotype[11,12,38]. The protection of macrophages from mitochondrial iron overload leads to an anti-inflammatory phenotype of these cells under both chow dox and HFD dox conditions (Fig. 8p). This result is in line with previous studies showing that an iron cycling phenotype is related to an anti-inflammatory M2-like signature[11,12,38]. In contrast, mitochondrial iron overload in macrophages achieved by FTMT overexpression leads to opposite effects on iron metabolism by increasing iron uptake and storage. The dysregulation of iron release from macrophages exacerbates iron sequestration and contributes to a less dynamic iron cycling phenotype than observed with MitoNEET overexpression. This increase in iron storage also promotes pro-inflammatory properties in macrophages. Our results thus highlight the importance of mitochondrial iron content in the regulation of macrophage polarization and function.

Iron-dependent immunometabolic regulation of macrophage function

Macrophage polarization is highly dependent on their metabolic state[40]. M1-like macrophages are often considered predominantly glycolytic, while M2-like macrophages are considered oxidative[41,42]. However, M1-like macrophages also require a constant supply of tricarboxylic acid cycle intermediates, for instance to produce cytokines such as interleukin (IL)-1β[42,43]. In M2-like macrophages, the tricarboxylic acid cycle is highly active and respiration is coupled efficiently in the electron transport chain, which maintains enhanced oxidative phosphorylation while curbing ROS production[44–46]. In mitochondria, the different complexes that are part of the electron transport chain are not only heavily dependent on iron availability and Fe–S cluster biogenesis, but also the center for ROS production during obesity[20–23]. The influence mitochondrial iron thus exerts on both the

energetic and oxidative status of macrophages explains the central role its availability has in shaping cell polarization.

Interestingly, in our study, both mitochondrial iron depletion and overload lead to a lower mitochondrial metabolism. Many studies have shown that iron chelation in macrophages decreases oxidative metabolism, thereby protecting from pro-inflammatory overstimulation[23,42,47,48]. We demonstrate that preventing macrophage mitochondrial iron overload not only decreases mitochondrial activity, but also promotes an anti-inflammatory cellular state. The diminished mitochondrial metabolism is mainly due to reductions in complex I, II and III of the electron transport chain, which are enriched in Fe–S cluster-bearing proteins. Inhibition of ROS production from complex I of the electron transport chain with metformin or rotenone, activating pyruvate kinase 2 (PKM2) with DASA-58 or TEPP-46, or activation of adenosine monophosphate-activated protein kinase (AMPK) with 5-aminoimidazole-4-carboxamide ribonucleotide (AICAR) has been shown to influence the class switching of macrophages from M1-like to M2-like in a similar manner[49–51]. Moreover, increased complex II activity has been proposed to be responsible for the activation of M1-like macrophages and accumulation of succinate, also promoting IL-1β production[18,42,52,53]. Decreased complex II activity, in turn, results in reduced IL-1β production[42], a phenomenon that we observed here as well. In line with published works, we demonstrate that the expression levels of Fe–S cluster-enriched complexes such as complex I, II and III decrease in response to MitoNEET overexpression, resulting in attenuated ROS production and lipid peroxidation in adipose tissue. However, while we observe that excessive mitochondrial iron accumulation in macrophages results in decreased mitochondrial activity, it promotes a pro-inflammatory cellular state. Excess iron has previously been shown to react with oxygen in the Fenton reaction, contributing to ROS production in many cell types, which can trigger a distinct form of cell death referred to as ferroptosis[54,55].

Our observations related to the metabolic reprogramming of macrophages provide new insights into the interconnection of mitochondrial function and immune cell activity. We furthermore reveal that selectively manipulating mitochondrial iron levels in macrophages can exert immediate effects on the iron metabolism of surrounding cells, such as adipocytes, as well.

Adipose tissue macrophages as sensors and regulators of adipose tissue iron metabolism

Comparable to macrophages, iron also shapes the function of adipocyte[38]. In line with previous studies, we confirm that adipocytes become overloaded with iron during obesity, concomitant with a reduced iron content in macrophages[11,16,25,56]. Fine-tuning the iron content in adipose tissue is crucial for its proper function during obesity and prevents systemic metabolic dysregulation[13,27,30]. Sufficient iron levels are needed to facilitate adipogenesis and adipocyte lipid handling but must not exceed an upper threshold, or else insulin sensitivity deteriorates[13,16,27,30,57]. Interestingly, strategies to reduce systemic iron concentrations such as consumption of a low-iron diet, chelation therapy or phlebotomy improve systemic insulin sensitivity in animal models[56,58,59] and humans with obesity[16,32,60,61]. The benefits of iron deprivation have also been attributed

to a reduction of inflammation in macrophages[42,48]. Our study supports that protecting ATMs from mitochondrial iron overload during obesity reduces adipocyte iron overload. As a result, adipocyte ROS production is limited, and adipocyte function is preserved. Iron is also indispensable for mitochondrial biogenesis and function[13,27,30]. We demonstrate that mitochondrial iron depletion from ATMs can directly improve mitochondrial activity and adiponectin production in adipocytes. In contrast, mitochondrial iron overload in ATMs results in a drastic increase in adipocyte iron content, also impinging on adiponectin production. That macrophage iron overload can directly promote local inflammation and deterioration of adipose tissue function is fully in line with observations made by others[16,38,62].

Our study illustrates the extent to which mitochondrial iron overload results in deleterious metabolic outcomes such as glucose intolerance and insulin resistance. Beyond this, we establish that targeted depletion of iron from ATM mitochondria is capable of reversing obesity and the metabolic deterioration associated with it.

Proposed mechanism

The cross-talk between macrophages and adipocytes influences the progression of obesity and metabolic disorders. Cytokines are prime candidates mediating this cross-talk. Our study exposes both iron-dependent and iron-independent effects that ATMs have on surrounding adipocytes. To our knowledge, no previous studies have addressed the direct links existing between ATM and adipocyte iron metabolism. Of note though, other studies have demonstrated the impact of anti-inflammatory cytokines on the iron content and polarization of ATMs to M2-like macrophages. As such, IL-13 and IL-4 have been shown to constitute key regulators of macrophage iron metabolism, reducing the LIP in these cells[63,64]. In our study, IL-4 and IL-13 were upregulated by mitochondrial iron depletion and downregulated by mitochondrial iron overload. These two cytokines may partially explain the decrease in LIP we observed in adipocytes from Mac-MitoNEET^{TG} eWAT. Pro-inflammatory cytokines such as interferon-γ, IL-6 and tumour necrosis factor have in turn been shown to promote iron overload in macrophages by altering ferritin and transferrin receptor expression[64–66]. We can speculate that the pro-inflammatory factors that were upregulated in our study may have had effects on adipocytes as well, promoting their overloading with iron in the context of obesity[63,64].

Another type of mediator relaying information between ATMs and adipocytes are metabolites. In our study, we demonstrate that both Mac-MitoNEET^{TG} and Mac-Ftmt^{TG} ATMs exhibit a reduction in mitochondrial metabolism. However, details differ between the two models. While Mac-MitoNEET^{TG} ATMs display a decrease in complex I, II and III, Mac-Ftmt^{TG} ATMs display a decrease in complex V alone. It is fair to assume that the differential regulation of mitochondrial respiration in these two models will also result in distinct shifts in metabolite abundance. Studies show that activation of macrophages evoked pronounced alterations in their metabolite profile[49,67]. Activating macrophages with lipopolysaccharides for instance leads to increased lactate and pyruvate release. Further metabolomic studies will need to be performed to evaluate differences in the metabolite

abundance in Mac-MitoNEET^{TG} and Mac-Ftmt^{TG} ATMs and to identify candidates capable of affecting adipocyte metabolism.

Iron itself constitutes another candidate in the cross-talk between ATMs and adipocytes. Iron deficiency has been associated with obesity and related metabolic disorders[15]. Under these very same conditions of low systemic iron levels, tissues such as WAT are oversaturated with iron[68]. Obesity is accompanied by a dysregulation of iron cycling in tissues[38]. The cycling of iron in ATMs overexpressing MitoNEET leads to a dynamic turnover of iron in WAT. This turnover may contribute to a re-exposure of adipocytes to iron locally in WAT that may stimulate them to metabolize it. Our and other studies show that adipocytes respond to an iron exposure by increasing iron release, an ability that is lost with obesity. Moreover, treating adipocytes with conditioned medium from Mac-MitoNEET^{TG} ATMs promotes the release of iron. This results in increased iron concentrations in the conditioned medium, which, in synergy with anti-inflammatory cytokines, may protect adipocytes from iron overload and its deleterious consequences.

In summary, ATMs can produce a variety of factors that can influence adipocyte and adipose tissue homeostasis. Several non-mutually exclusive scenarios are conceivable as to how these factors operate. These scenarios encompass not only direct interactions between ATMs and adipocytes, but also indirect interactions involving other local cell types including immune, endothelial and progenitor cells. Future investigations will evaluate which factors from ATMs help to shape iron metabolism in adipocytes.

Methods

Mouse models

All animal experimental protocols were approved by the Institutional Animal Care and Use Committees of the University of Texas Southwestern (UTSW) Medical Center (protocol no. 2015–101207) and West Virginia University (protocol no. 190102017).

We established two mouse models with dox-inducible, macrophage-selective mitoNEET or Ftmt overexpression by crossing *TRE*-mitoNEET or *TRE*-Ftmt mice with *Csfr1*-rtTA mice[13,27,28,30]. MitoNEET$^{flox/flox}$ (*Cisd1*$^{flox/flox}$) mice were generated by Applied StemCell using CRISPR–Cas9 technology to insert loxP sequences into intron 1 and intron 2 for the *Cisd1* gene of C57BL/6J mice. These mice were bred with wild-type C57BL/6J mice and subsequent litters were tested by PCR genotyping and Sanger sequencing. The genotyping primers for the insertion of the 5' loxP site were: 5′-CTT TAG GCA CCA GTA GAG GGT GTC AG-3′ and 5′-CAC GAG TAT GAA GAG CTG TGT GTG CTG G-3′. The wild-type band was 301 bp and the loxP band was 335 bp in size. Then, to establish a dox-inducible, macrophage-specific mitoNEET knockout model, mitoNEET$^{flox/flox}$ mice were crossed with *Csfr1*-rtTA and *TRE*-Cre mice (JAX strain, 006234).

Mice were housed under barrier conditions on a 12-h light/dark cycle in a temperature-controlled environment (22°C) with free access to food and water and constant veterinary supervision. Water and cages were autoclaved and cages were changed every other week.

The mouse genotype did not cause visible changes in initial weight, overall health or immune status.

All animals used in this study were littermate-controlled male mice and on a pure C57BL/6J background. Only male mice were used as female mice are more resistant to develop obesity and type 2 diabetes. The age and number of the mice used for the experiments are indicated for each experiment. To ensure reproducibility, two separate cohorts of mice were used whenever possible. No inclusion or exclusion criteria were applied, and the experiments were not randomized. No statistical method was used to predetermine the sample size for experiments.

Mice were maintained on a standard rodent chow diet (no. 5058, LabDiet) unless otherwise stated. Diet studies were initiated at 6 weeks of age. For Dox induction in chow-fed mice, a pellet chow diet (600 mg per kg; diet weight, no. S4107, Bio-Serv) was utilized. For HFD studies with no dox, mice were fed a diet with 60% calories from fat (no. D12492, Research Diets). In HFD-challenge experiments with dox induction, mice were fed a paste diet containing 60% calories from fat supplemented with 600 mg per kg (diet weight) dox (no. S7067, Bio-Serv). In all experiments involving chow dox or HFD dox feeding, the same diet was provided to all mice, including controls (that is, mice lacking the inducible transgenes *TRE*-mitoNEET, *TRE*-Mitoferritin or *TRE*-Cre).

Body composition analysis

Body fat and lean mass were measured in conscious mice using an EchoMRI-100 system (4-in-1, EchoMRI).

Triglyceride clearance test

Mice were fasted overnight for 16 h before administration of 15 μl per gram body weight of 20% Intralipid (Sigma-Aldrich) by gastric gavage. Blood was collected from the tail vein at 0, 1, 2, 3, 4 and 6 h and assayed for triglycerides using the Infinity Triglycerides Reagent (Thermo Fisher Scientific).

Oral glucose tolerance test

Mice were fasted for 4 h before administration of 2.5 gram per kilogram body weight of glucose by gastric gavage. Blood was collected from the tail vein at 0, 15, 30, 60 and 120 min, and serum was obtained by centrifugation and stored frozen until further measurements. During the test, blood glucose concentrations were measured using Bayer Contour glucometers. Serum insulin was measured using the Ultra-Sensitive Mouse Insulin ELISA (Crystal Chem, 90080).

Indirect calorimetry

Parameters of energy intake and expenditure were measured in metabolic cages using the TSE Phenomaster climate-controlled indirect calorimetry system (TSE Systems).

Insulin tolerance test

Mice were fasted for 4 h before administration of 0.75 U per kg body weight of human insulin (Humulin R) by intraperitoneal injection. Blood was collected from the tail vein at 0, 15, 30, 60 and 120 min and blood glucose concentrations were measured using Bayer Contour glucometers.

RNA isolation, reverse transcription and quantitative RT–PCR

RNA was isolated from cells snap-frozen using the RNAqueous-Micro Total RNA Isolation Kit (Thermo Fisher Scientific). RNA was quantified on a NanoDrop Spectrometer (Thermo Fisher Scientifc). cDNA was prepared by reverse transcription using the iScript cDNA Synthesis Kit (Bio-Rad). RT–qPCR was performed using PowerUp SYBR Green Master Mix (Thermo Fisher Scientific) on a QuantStudio 6 Flex system (Thermo Fisher Scientific). Ct values for quantitative PCR data were calculated by QuantStudio Real-Time PCR software (version 1.2, Applied Biosystems). Data were analysed using the threshold cycle (Ct) method with *B2M* gene expression for normalization. mRNA expression levels were calculated using the ΔΔCt method as described previously[69]. Primer sequences are listed in Supplementary Table 3.

Histology

Tissues were collected, fixed in 10% PBS-buffered formalin for 24 h at room temperature, and stored in 50% ethanol at room temperature. Following paraffin embedding and sectioning at 5 μm, tissues were stained with H&E.

Isolation of floated adipocytes and stromal-vascular fraction

The dissociation of adipose tissue was adapted from work by Peics et al.[70]. In brief, WAT samples from male mice from the indicated strain were minced with scissors in Hank's balanced salt solution containing 1.5% BSA (Sigma-Aldrich) and 1 mg ml^{-1} collagenase D (Roche). For both epididymal and subcutaneous adipose tissue, two pads were combined. Minced samples were incubated for 45 min (epididymal) or 80 min (subcutaneous) at 37°C in a shaking water bath at 100 rpm. Samples were mixed every 20 min by gentle pipetting to allow the tissue to digest equally. The samples were filtered through a 100 μm cell strainer, cold PBS + 2% FBS was added to dilute the digestion buffer, and the samples were centrifuged for 5 min at 600*g* and 4°C to pellet the SVF. Floating adipocytes were collected, the remaining supernatant was discarded and the pelleted cells were resuspended in Red Blood Cell Lysis Buffer (Sigma-Aldrich). Lysis was stopped by addition of PBS + 2% FBS, the samples were filtered through a 40-μm cell strainer and centrifuged for 5 min at 600*g* and 4°C to pellet the cells. The pelleted cells were either cultured or analysed by flow cytometry as described below.

Flow cytometry and fluorescence-activated cell sorting

Cells were analysed and sorted on BD Biosciences LSRFortessa SORP and BD Biosciences FACS Aria Fusion instruments, respectively, at the Children's Medical Center Research Institute Flow Core at UTSW. Antibodies used for flow cytometry were: Purified Rat Anti-mouse CD16/CD32 FC Block clone 2.4G2 (BD Biosciences, 553142); FITC CD45

clone 30-F11 (BD Biosciences, 553080); FITC CD31 clone 390 (BD Biosciences, 558738); PE-CF594 anti-F4/80 clone T45–2342 (BD Biosciences, 565613); BB700 anti-CD11b clone M1/70 (BD Biosciences, 566417); BV421 anti-CD11c clone (BD Biosciences, 565452); and Alexa Fluor 647 anti-CD206 clone MR5D3 (BD Biosciences, 565250). Data were analysed using FlowJo software (version 9, BD).

Cells isolated from eWAT were first blocked for 10 min at 4°C in PBS + 2% FBS supplemented with anti-mouse CD16/CD32 Fc Block (clone 2.4G2; 1:200 dilution) and then stained for 20 min at 4°C in PBS + 2% FBS supplemented with the according primary antibodies. SVF cells were stained with FITC anti-CD45 (clone 30-F11; 1:200 dilution), PE-CF594 anti-F4/80 (clone T45–2342; 1:200 dilution), BB700 anti-CD11b (clone M1/70; 1:200 dilution), AF647 anti-CD206 (clone MR5D3; 1:200 dilution) and BV421 anti-CD11c (clone N418; 1:200 dilution). Stained cells were then washed once with cold PBS + 2% FBS and centrifuged for 5 min at 600*g* and 4°C.

For flow cytometry analyses only, cells were fixed using BD Cytofix for 20 min at 4°C. After fixation, cells were centrifuged for 5 min at 600*g* and 4°C and resuspended in cold PBS + 2% FBS.

For FACS, cells were filtered through a cell-strainer cap into a polystyrene round-bottom tube and sorted into 100% FBS. Sorted cells were either cultured or centrifuged and resuspended in lysis solution for RNA isolation described above.

Gating strategy

The gating strategy is described in Supplementary Fig. 1. Live cells were selected on a forward scatter area (FSC-A)/side scatter area (SSC-A) plot. Singlets were selected on subsequent forward scatter width (FSC-W) and side scatter width (SSC-W) plots. Unstained cells isolated from wild-type mice were used to determine background fluorescence levels. Cell subpopulations can be distinguished on the basis of different cell surface markers. For macrophages, FITC anti-CD45 was used to select haematopoietic cells and PE-CF594 anti-F4/80 as well as BB700 anti-CD11b to select macrophages ($F4/80^+$ $CD11b^+$ Mac; versus $F4/80^-$ $CD11b^-$ non-Mac). Within the macrophage population, M1-like pro-inflammatory macrophages and M2-like anti-inflammatory macrophages were distinguished as BV421 anti-CD11c (M1) and AF647 anti-CD206 (M2).

Stromal-vascular fraction cell culture and adipocyte differentiation

Freshly isolated SVF cells from subcutaneous adipose tissue from male mice from the indicated strain were cultured at 37°C and 10% CO_2 in SVF growth medium consisting of DMEM/F12 (Thermo Fisher Scientific) supplemented with 10% FBS (Merck Millipore), 1% penicillin–streptomycin (Thermo Fisher Scientific) and 0.1% gentamycin (Thermo Fisher Scientific). Adipogenic differentiation was induced at confluence by addition of SVF growth medium supplemented with 500 µM 3-isobutyl-1-methylxanthine, 1 µM dexamethasone and 5 µg ml^{-1} insulin for 2 d. Following induction, the medium was replaced with fresh SVF growth medium supplemented with 5 µg ml^{-1} insulin every 2 d until 6–8 d after induction.

Where indicated, the cells were exposed for 1 d to macrophage-conditioned medium as well as either 400 μM of FAC or 100 μM of the iron chelator DFO as previously described by refs. [42,48,71,72].

Peritoneal macrophage isolation

Male mice were intraperitoneally injected with 3 ml of 2% thioglycolate solution. After 3 d, the mice were euthanized and their abdominal wall was exposed. The peritoneal cavity was injected with 5 ml of cold PBS + 2% FBS, the abdomen was massaged for 1 min, and the cell suspension containing the peritoneal macrophages was aspirated from the peritoneal cavity. The aspirate was centrifuged for 5 min at 600*g* and 4°C. The pelleted cells were resuspended in 10 ml PBS, centrifuged again for 5 min at 600*g* and 4°C and then then either analysed immediately or cultured.

Macrophage cell culture

ATMs and peritoneal macrophages were cultured at 37°C and 5% CO_2 in macrophage growth medium consisting of RPMI 1640 medium (Thermo Fisher Scientific) supplemented with 10% FBS (Merck Millipore) and 1% penicillin–streptomycin (Thermo Fisher Scientific). The medium was renewed the day after initial seeding. Dox treatment was performed at a concentration of 4.4 μM[13].

Iron measurements

Total iron and copper concentrations in macrophages and adipocytes were determined by ICP-MS at the Iron and Heme Core Facility at the University of Utah. Free iron concentrations (LIP) were determined using the QuantiChrom Iron Assay Kit (BioAssay Systems). In preparation of free iron measurements, macrophages or adipocytes were lysed in PBS + 1% Triton X-100 for 15 min on ice and samples were cleared from cellular debris by centrifugation for 15 min at 13,000*g* and 4°C. Total and free iron concentrations were normalized to protein concentrations in the same samples.

Extracellular flux analyses

All assays were performed on an Agilent Seahorse XFe24 Extracellular Flux Analyser. Mitochondrial respiration data were viewed and analysed through the Wave software (version 2.6.0, Agilent). The day before analysis, cells were counted and seeded into Agilent Seahorse XF24 cell culture microplates at a density of 60,000 cells per well in 300 μl of macrophage growth medium. The cells were cultured overnight at 37 °C and 10% CO_2. In parallel, an Agilent Seahorse XFe24 extracellular flux assay plate was calibrated in Seahorse XF Calibrant Solution overnight at 37°C without CO_2 supplementation.

Mitochondrial stress assay

On the day of the assay, the cells were rinsed with mitochondrial assay medium consisting of Agilent Seahorse XF RPMI medium, pH 7.4, supplemented with 1 mM sodium pyruvate, 2 mM GlutaMAX (Thermo Fisher Scientific) and 7 mM glucose and then incubated in 625 μl of assay medium for 1 h at 37°C without CO_2 supplementation. The modulators oligomycin (10 mM), FCCP (10 mM) and rotenone + antimycin-A (1 mM each) were

diluted in assay medium and loaded into the ports of the Seahorse XFe24 extracellular flux assay plate as follows: 75 µl of oligomycin in port A (1 µM concentration in the well after injection), 83 µl of FCCP in port B (4 µM after injection) and 93 µl rotenone + antimycin-A in port C (150 nM each after injection). The measurement was performed as follows: basal three cycles of 3 min mixing, 0 min waiting, 3 min measuring > oligomycin injection followed by three cycles > FCCP injection followed by 5 cycles > rotenone + antimycin-A injection followed by three cycles[13].

Glycolysis stress assay

On the day of the assay, the cells were rinsed with glycolysis assay medium consisting of Agilent Seahorse XF RPMI medium, pH 7.4, supplemented with 2 mM GlutaMAX (Thermo Fisher Scientific) without added sodium pyruvate or glucose and then incubated in 625 µl of assay medium for 1 h at 37°C without CO_2 supplementation. The modulators glucose (20 mM), oligomycin (1 µM) and 2-deoxyglucose (2-DG; 100 mM) were diluted in assay medium and loaded into the ports of the Seahorse XFe24 extracellular flux assay plate as follows: 80 µl of glucose in port A (2.6 mM after injection), 80 µl of oligomycin in port B (120 nM after injection) and 80 µl of 2-DG in port C (12.8 mM after injection). The measurement was performed as follows: basal three cycles of 3 min mixing, 0 min waiting, 3 min measuring > glucose injection followed by three cycles > oligomycin injection followed by three cycles > 2-DG injection followed by three cycles[13].

Western blotting

Protein was extracted from cells by homogenization in RIPA buffer supplemented with protease inhibitors (Pierce; Thermo Fisher Scientific). Protein concentrations were determined using the Pierce BCA Protein Assay Kit (Thermo Fisher Scientific). Proteins were resolved in MES buffer on Novex 4–12% Bis-Tris gels (Thermo Fisher Scientific) and transferred to nitrocellulose membranes using the Bio-Rad Trans-Blot Turbo system. The blots were then blocked with 5% BSA for 1 h at room temperature and then incubated with primary antibodies diluted in blocking buffer overnight at 4°C. The following antibodies were used: Rabbit polyclonal anti-mouse MitoNEET homemade (1:1,000 dilution)[27], anti-OXPHOS Rodent antibody cocktail (1:1,000 dilution; Abcam, ab110413, rat heart tissue lysate as positive control), anti-CD163 (1:1,000 dilution; Abcam, 182422), anti-CD91 (1:3,000 dilution; a generous gift from J. Herz (UTSW)). Anti-Prohibitin antibody-Mitochondrial Marker (1:1,000 dilution; Abcam, ab28172), Monoclonal Anti-β-Actin antibody (1:10,000 dilution; Sigma-Aldrich, A5441), FtMT/mitochondrial ferritin (Sigma, SAB2700108), anti-Ferroportin (1:1,000 dilution; NBP1–21502, Novus Biologicals), glyceraldehyde 3-phosphate dehydrogenase (1:1,000 dilution; Cell Signaling Technology, 5174) and FTH1/ferritin heavy chain (1:1,000 dilution; Cell Signaling Technology, 4393S). Primary antibodies were detected using secondary antibodies labelled with infra-red dyes emitting at 700 nm or 800 nm: IR-Dye 800CW Donkey antibody against rabbit (Li-Cor, 92632213); IR-Dye 800CW Goat antibody against Mouse (Li-Cor, 92632210); and IR-Dye 680RD Donkey antibody against Mouse (Li-COR, 92668072). Secondary antibody staining was performed at a 1:10,000 dilution for 1 h at room temperature. The blots were then scanned on a Li-Cor Odyssey instrument (Li-Cor Bioscience). Western blot band intensity

was collected by Li-Cor Odyssey Imager software (version 3.0, LI-COR) and analysed using ImageJ.

Mitochondria isolation

Cells were disrupted in ice-cold isolation buffer consisting of 210 mM mannitol, 70 mM sucrose, 5 mM HEPES, 1 mM EGTA and 0.5% BSA using a Potter-Elvehjem homogenizer. The homogenate was centrifuged for 10 min at 600*g* and 4°C. The resulting supernatant was filtered through cheesecloth and centrifuged for 15 min at 10,000*g* and 4°C to pellet mitochondria. The final supernatant was concentrated using Amicon Ultra 0.5 ml centrifugal filters (Millipore/Sigma) and used for cytosolic fraction measurements.

Protein carbonylation assay

Cells were homogenized in cold buffer containing 100 mM sodium acetate, 20 mM NaCl, 100 μM EDTA and 100 μM PMSF, pH 5.5. Following lysis, Triton X-100 was added to each sample to a final concentration of 1% and the samples were incubated for 20 min on ice. Homogenates were cleared by centrifugation for 10 min at 16,000*g* and 4°C. Protein concentrations of the supernatants were determined and 50 μg of protein was supplemented with 500 μM EZ-Link hydrazide-biotin. The samples were incubated for 2 h at room temperature, after which the reaction was stopped by addition of western blot sample loading buffer (Li-Cor) without any reducing agent. Proteins were allowed to denature for 20 min at room temperature and then separated on Novex 4–12% Bis-Tris gels (Thermo Fisher Scientific) and transferred to nitrocellulose membranes using the Bio-Rad Trans-Blot Turbo system. Detection of biotin-modified protein was accomplished using 800W-labelled streptavidin beads (Thermo Fisher Scientific). The blots were re-probed with anti-GAPDH to check for equal loading.

No statistical method was used to predetermine sample size. The experiments were not performed blinded. Data are displayed as the mean ± s.e.m. All statistical analyses were performed using Prism 7.04 (GraphPad Software). Differences between multiple conditions and two groups over time were evaluated using two-way ANOVA with Sidak's post hoc test for multiple comparisons. For comparisons between several different groups, a Kruskal–Wallis test (one-way ANOVA) with Dunn's post hoc test for multiple comparisons was used. For comparisons between two independent groups, a Student's *t*-test was used. For cell culture experiments, each biological replicate corresponds to a cell preparation from separate mice. For mouse experiments, each biological replicate corresponds a separate mouse.

Reporting summary

Further information on research design is available in the Nature Research Reporting Summary linked to this article.

Extended Data

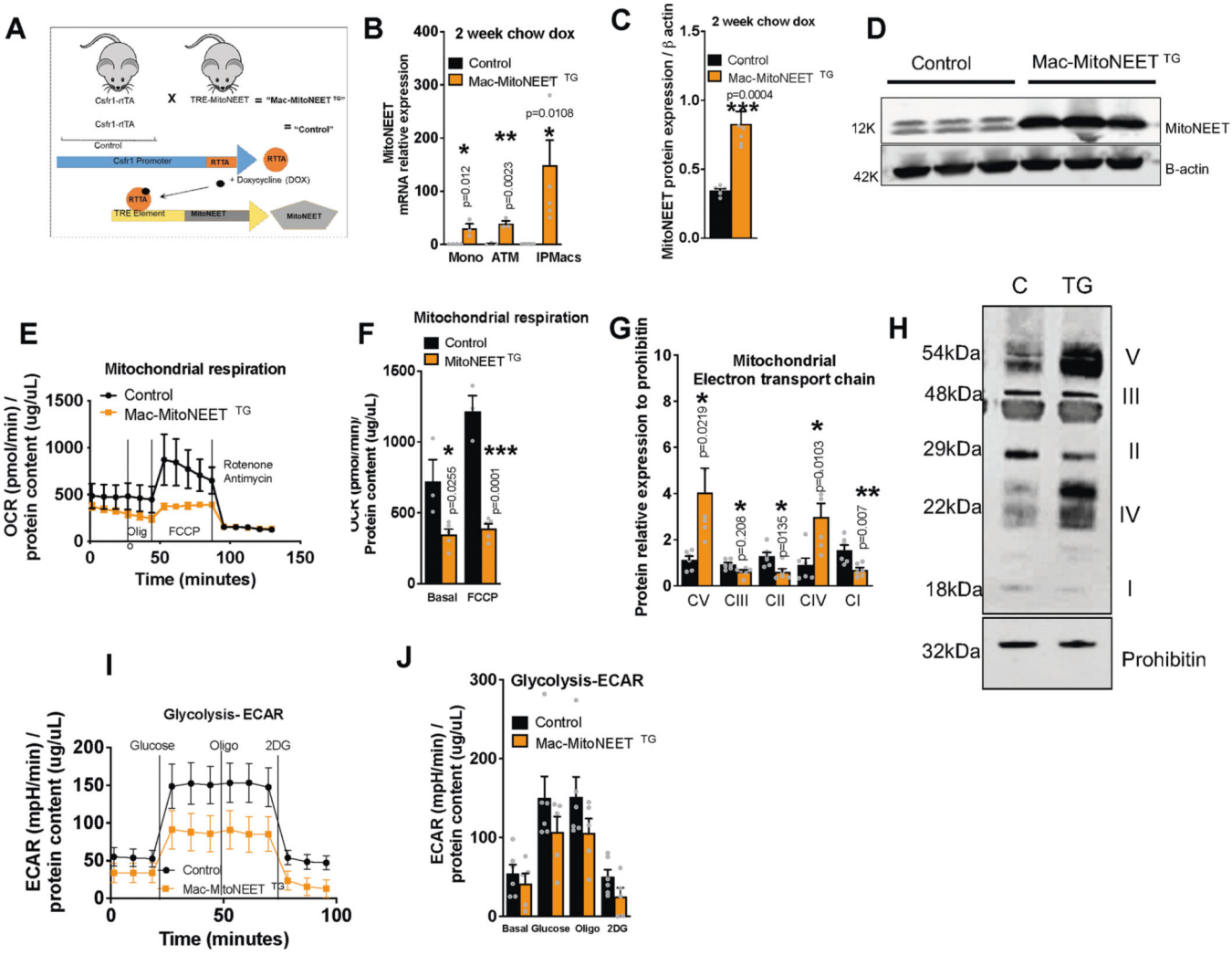

Extended Data Fig. 1 |. Validation of MitoNEET overexpression in macrophages.

(a-j) Six-week-old male control and Mac-MitoNEET^{TG} mice were fed chow dox for 2 weeks. **(a)** Breeding strategy. **(b)** *Cisd1* mRNA levels relative to control in monocytes (control n = 4, TG n = 3), ATMs (n = 3), and peritoneal macrophages (n = 6). **(c)** MitoNEET protein expression relative to β-actin in peritoneal macrophages (n = 6). **(d)** Representative Western blots chosen from 2 independent experiments. **(e-f)** Mitochondrial respiration in peritoneal macrophages (control n = 3, TG n = 5). **(g)** Mitochondrial electron transport chain protein expression relative to prohibitin in peritoneal macrophages (n = 6). **(h)** Representative Western blots. **(i-j)** Glycolysis stress test in peritoneal macrophages (control n = 6, TG n = 6). Significance in **(b-c, f-g, j)** between control and Mac-MitoNEET^{TG} was calculated using a two-tailed Student's t-test. Significance in **(e, i)** was calculated using a 2-way ANOVA with Sidak's post-test for multiple comparisons. Error bars represent mean ± S.E.M. * (P < 0.05), ** (p < 0.01), *** (p < 0.0001), **** (p < 0.00001).

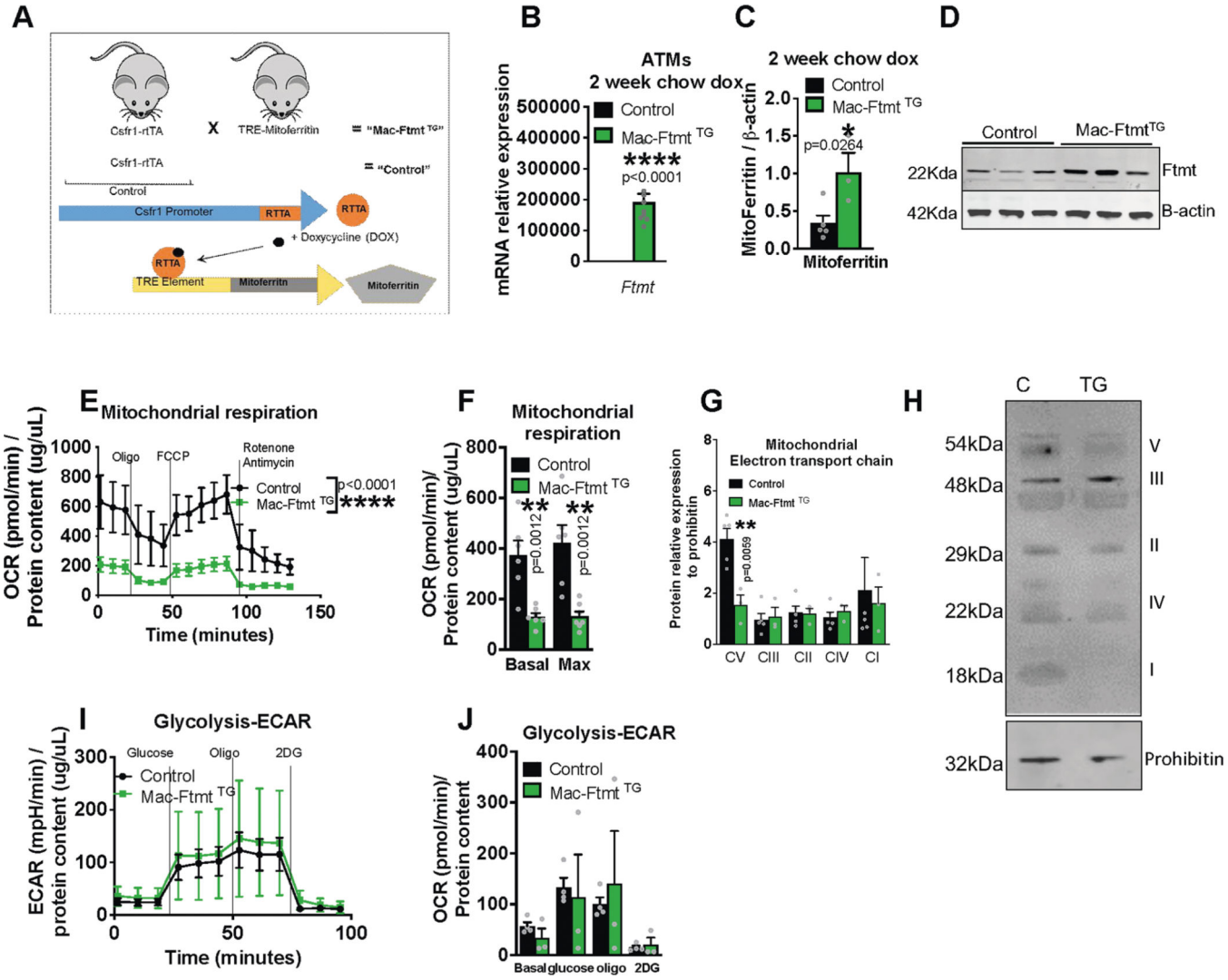

Extended Data Fig. 2 |. Validation of Ftmt overexpression in macrophages.

(a-j) Six-week-old male control and Mac-Ftmt^{TG} mice were fed chow dox for 2 weeks. **(a)** Breeding strategy. **(b)** *Ftmt* mRNA levels relative to control in peritoneal macrophages (control n = 7, TG n = 9). **(c)** FTMT protein expression relative to β-actin in peritoneal macrophages (control n = 5, TG n = 3). **(d)** Representative Western blots chosen from 2 independent experiments. **(e-f)** Mitochondrial respiration in peritoneal macrophages (control n = 6, TG n = 7). **(g)** Mitochondrial electron transport chain protein expression relative to prohibitin in peritoneal macrophages (control n = 5, TG n = 3). **(h)** Representative Western blots (control n = 5, TG n = 3). **(i-j)** Glycolysis stress test in peritoneal macrophages (control n = 4, TG n = 3). Significance in **(b-c, f-g, j)** between control and Mac-Ftmt^{TG} was calculated using a two-tailed Student's t-test. Significance in **(e, i)** was calculated using a 2-way ANOVA with Sidak's post-test for multiple comparisons. Error bars represent mean ± S.E.M. * (P < 0.05), ** (p < 0.01), *** (p < 0.0001), **** (p < 0.00001).

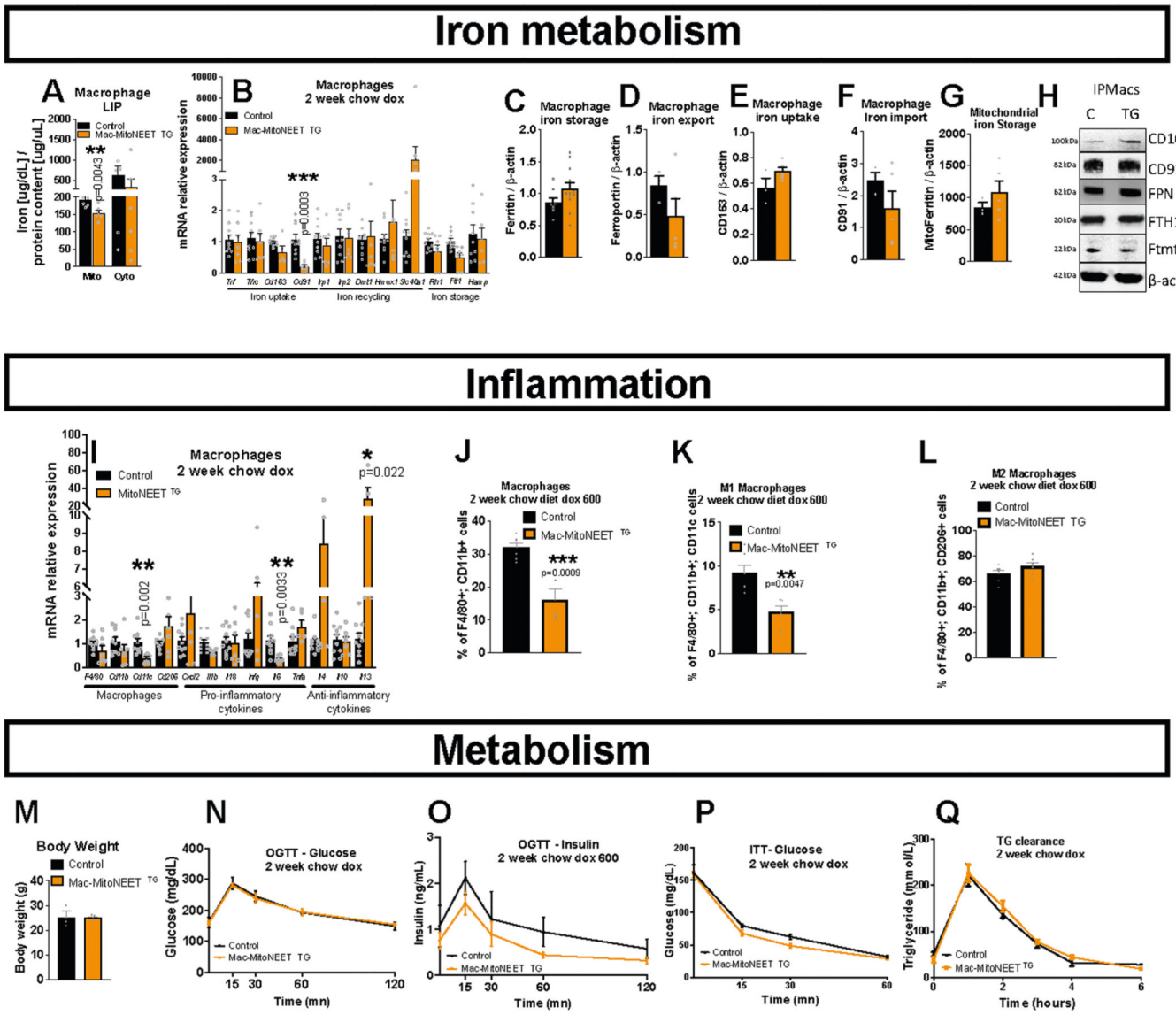

Extended Data Fig. 3 |. Macrophages respond to mitoNEET overexpression by up-regulating iron storage.

(a-q) Male control and Mac-MitoNEET^{TG} mice were fed chow dox for 2 weeks. **(a)** Labile iron pool (LIP) in mitochondrial and cytosolic compartments of peritoneal macrophages (control n = 7, TG n = 6). **(b)** mRNA levels of iron metabolism genes relative to control in peritoneal macrophages (control n = 10, TG n = 7). **(c)** Ferritin (control n = 9, TG n = 12), **(d)** Ferroportin (control n = 3, TG n = 5), **(e)** CD163 (control n = 3, TG n = 5), **(f)** CD91 (control n = 3, TG n = 5) and **(g)** FTMT (control n = 3, TG n = 5) protein expression relative to β-actin in peritoneal macrophages. **(h)** Representative Western blots chosen from 2 independent experiments **(i)** mRNA levels of inflammation markers relative to control in peritoneal macrophages (control n = 7, TG n = 10). **(j-l)** Flow cytometric measurement of total (control n = 6, TG n = 5), M1-like control n = 6, TG n = 5) and M2-like macrophages in eWAT (n = 6). **(m)** Body weight (control n = 3, TG n = 5). **(n-o)** Oral glucose tolerance test (control n = 3, TG n = 5). **(n)** Blood glucose levels. **(o)** Serum insulin levels. **(p)** Blood

glucose levels during insulin tolerance test (control n = 3, TG n = 5). **(q)** Serum triglyceride levels during triglyceride clearance (n = 6). Significance in **(a-g, i-m)** between control and Mac-MitoNEET^{TG} was calculated using a two-tailed Student's t-test. Significance in **(n-q)** was calculated using a 2-way ANOVA with Sidak's post-test for multiple comparisons. Error bars represent mean ± S.E.M. * (P < 0.05), ** (p < 0.01), *** (p < 0.0001), **** (p < 0.00001).

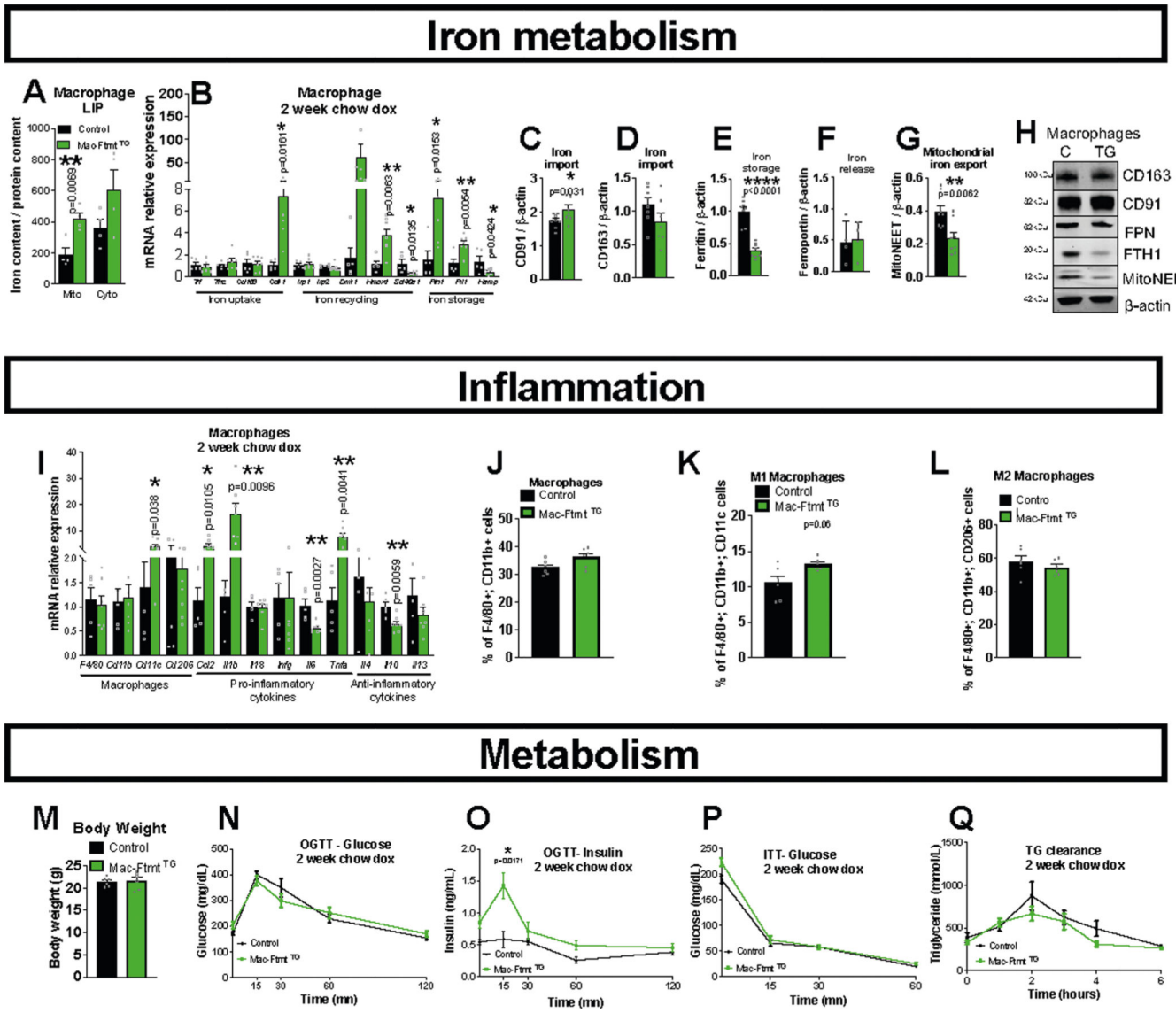

Extended Data Fig. 4 |. Macrophages respond to Ftmt overexpression by up-regulating iron uptake.

(a-q) Male control and Mac-Ftmt^{TG} mice were fed chow dox for 2 weeks. **(a)** Labile iron pool (LIP) in mitochondrial and cytosolic compartments of peritoneal macrophages (n = 4). **(b)** mRNA levels of iron metabolism genes relative to control in peritoneal macrophages (control n = 5, TG n = 7). **(c)** CD91 (n = 8), **(d)** CD163 (n = 8), **(e)** Ferritin (n = 8), **(f)** Ferroportin (n = 4) and **(g)** MitoNEET (n = 8) protein expression relative to β-actin in

peritoneal macrophages (n = 8). **(h)** Representative Western blots chosen from 2 independent experiments. **(i)** mRNA levels of inflammation markers relative to control in peritoneal macrophages (control n = 5; TG n = 7). **(j-l)** Flow cytometric measurement of total, M1-like and M2-like macrophages in eWAT (n = 6). **(m)** Body weight (n = 6). **(n-o)** Oral glucose tolerance test (n = 6). **(n)** Blood glucose levels (n = 6). **(o)** Serum insulin levels (control n = 7, TG n = 9). **(p)** Blood glucose levels during insulin tolerance test (control n = 6, TG n = 5). **(q)** Serum triglyceride levels during triglyceride clearance (n = 6). Significance in **(a-g, i-m)** between control and Mac-Ftmt^{TG} was calculated using a two-tailed Student's t-test. Significance in **(n-q)** was calculated using a 2-way ANOVA with Sidak's post-test for multiple comparisons. Error bars represent mean ± S.E.M. * ($P < 0.05$), ** ($p < 0.01$), *** ($p < 0.0001$), **** ($p < 0.00001$).

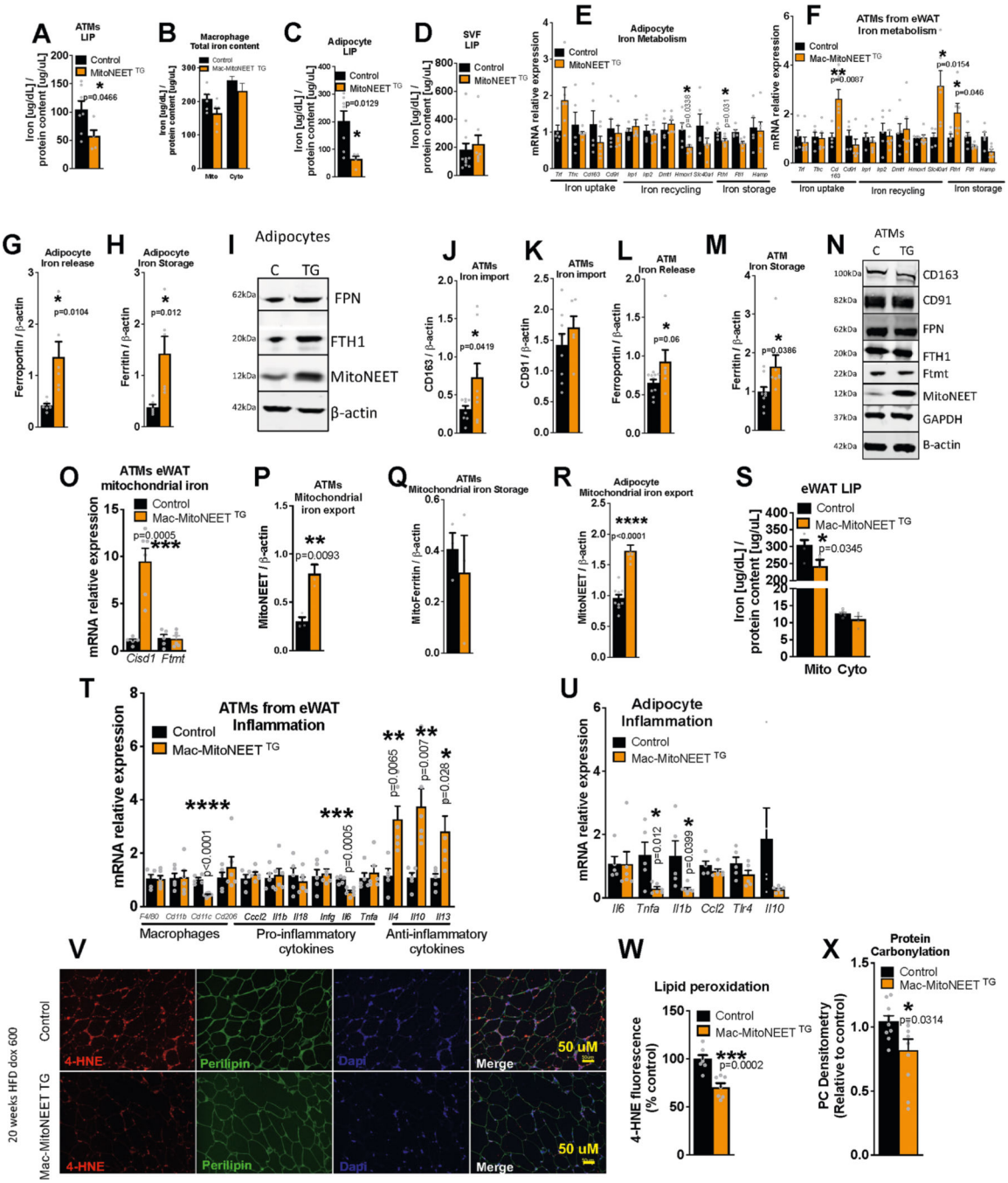

Extended Data Fig. 5 |. Mitochondrial iron depletion in macrophages during HFD increases iron recycling, protecting adipocytes from iron overload.

(a-x) Six-week-old male control and Mac-MitoNEET^{TG} mice were fed HFD dox for 6 weeks. **(a)** Labile iron pool (LIP) in ATMs from eWAT (control n = 7, TG n = 7) **(b)** Total iron content measured by ICP-MS in mitochondrial and cytosolic compartments in peritoneal macrophages (control n = 7, TG n = 5). **(c-d)** LIP in **(c)** adipocytes and **(d)** SVF from eWAT (control n = 7, TG n = 5). **(e-f)** mRNA levels of iron metabolism genes relative to control **(e)** adipocytes (control n = 5, TG n = 6) and **(f)** ATMs (control n =

6, TG n = 5) from eWAT. **(g)** Ferroportin and **(h)** Ferritin protein expression relative to β-actin in adipocytes from eWAT (n = 6). **(i)** Representative Western blots chosen from 2 independent experiments. **(j)** CD163 (n = 9), **(k)** CD91, **(l)** Ferroportin, and **(m)** Ferritin protein expression relative to β-actin in ATMs from eWAT (control n = 9, TG n = 6). **(n)** Representative Western blots chosen from 2 independent experiments. **(o)** mRNA levels of mitochondrial iron metabolism genes relative to control in ATMs from eWAT (control n = 5, TG n = 6). **(p)** MitoNEET and **(q)** Mitoferritin protein expression relative to β-actin in ATMs from eWAT (n = 3). **(r)** MitoNEET protein expression relative to β-actin in adipocytes from eWAT (control n = 9, TG n = 6). **(s)** LIP in mitochondrial and cytosolic compartments of eWAT (control n = 5, TG n = 4). **(t-u)** mRNA levels of inflammatory marker genes relative to control in **(t)** ATMs and **(u)** adipocytes from eWAT (control n = 5, TG n = 6). **(v)** Representative fluorescence microscopic images of 4-HNE, Perilipin and DAPI staining of eWAT chosen from 3 independent experiments. **(w)** Quantification of 4-HNE fluorescence in eWAT relative to control (control n = 8, TG n = 7). **(x)** Protein carbonylation in adipocytes from eWAT (control n = 10, TG n = 11). Significance in **(a-h, j-u, w-x)** between control and Mac-MitoNEET^{TG} was calculated using a two-tailed Student's t-test. Error bars represent mean ± S.E.M. * ($P < 0.05$), ** ($p < 0.01$), *** ($p < 0.0001$), **** ($p < 0.00001$).

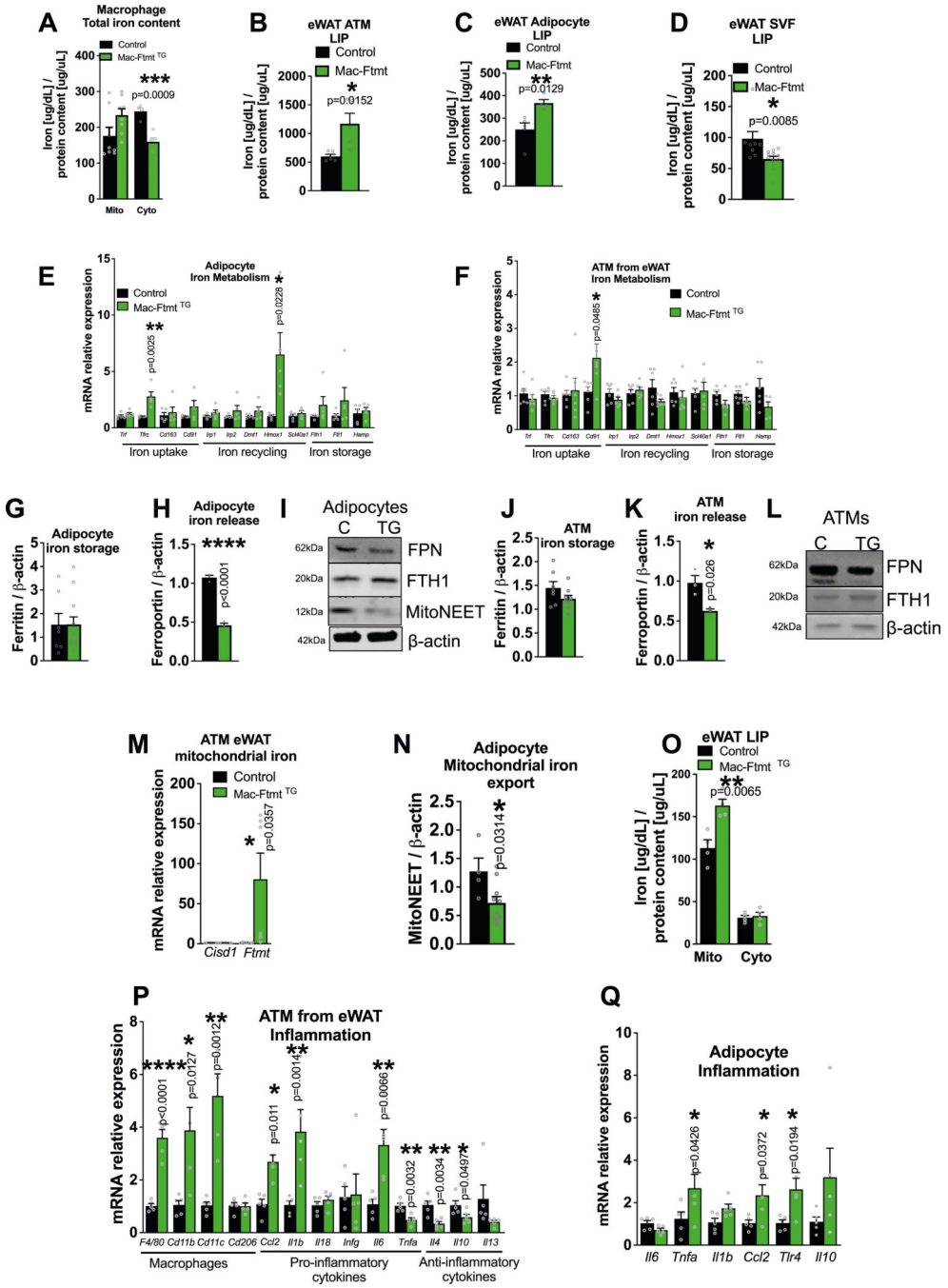

Extended Data Fig. 6 |. Mitochondrial iron overload in macrophages during HFD promotes adipocyte iron overload and inflammation.

(a-q) Six-week-old male control and Mac-Ftmt^{TG} mice were fed HFD dox for 6 weeks. **(a)** Total iron content measured by ICP-MS in mitochondrial (n = 8) and cytosolic (control n = 4, TG n = 5) compartments in peritoneal macrophages. **(b-d)** Labile iron pool (LIP) in **(b)** ATMs (control n = 4, TG n = 5), **(c)** adipocytes (control n = 9, TG n = 12) and **(d)** SVF (control n = 7, TG n = 5) from eWAT. **(e-f)** mRNA levels of iron metabolism genes relative to control in **(e)** adipocytes (n = 5) and **(f)** ATMs (n = 6) from eWAT. **(g)** Ferritin

(control n = 7, TG n = 12) and **(h)** Ferroportin (n = 3) protein expression relative to β-actin in adipocytes from eWAT. **(i)** Representative Western blots chosen from 3 independent experiments. **(j)** Ferritin (control n = 7, TG n = 9) and **(k)** Ferroportin protein expression relative to β-actin in ATMs from eWAT (n = 3). **(l)** Representative Western blots chosen from 3 independent experiments. **(m)** mRNA levels of mitochondrial iron metabolism genes relative to control in ATMs from eWAT (n = 6). **(i)** MitoNEET protein expression relative to β-actin in adipocytes from eWAT (control n = 4, TG n = 10). **(o)** LIP in mitochondrial and cytosolic compartments of eWAT (n = 4). **(p-q)** mRNA levels of inflammatory marker genes relative to control in **(p)** ATMs and **(q)** adipocytes from eWAT (n = 5). Significance in **(a-h, j-k, m-q)** between control and Mac-Ftmt^{TG} was calculated using a two-tailed Student's t-test. Error bars represent mean ± S.E.M. * ($P < 0.05$), ** ($p < 0.01$), *** ($p < 0.0001$), **** ($p < 0.00001$).

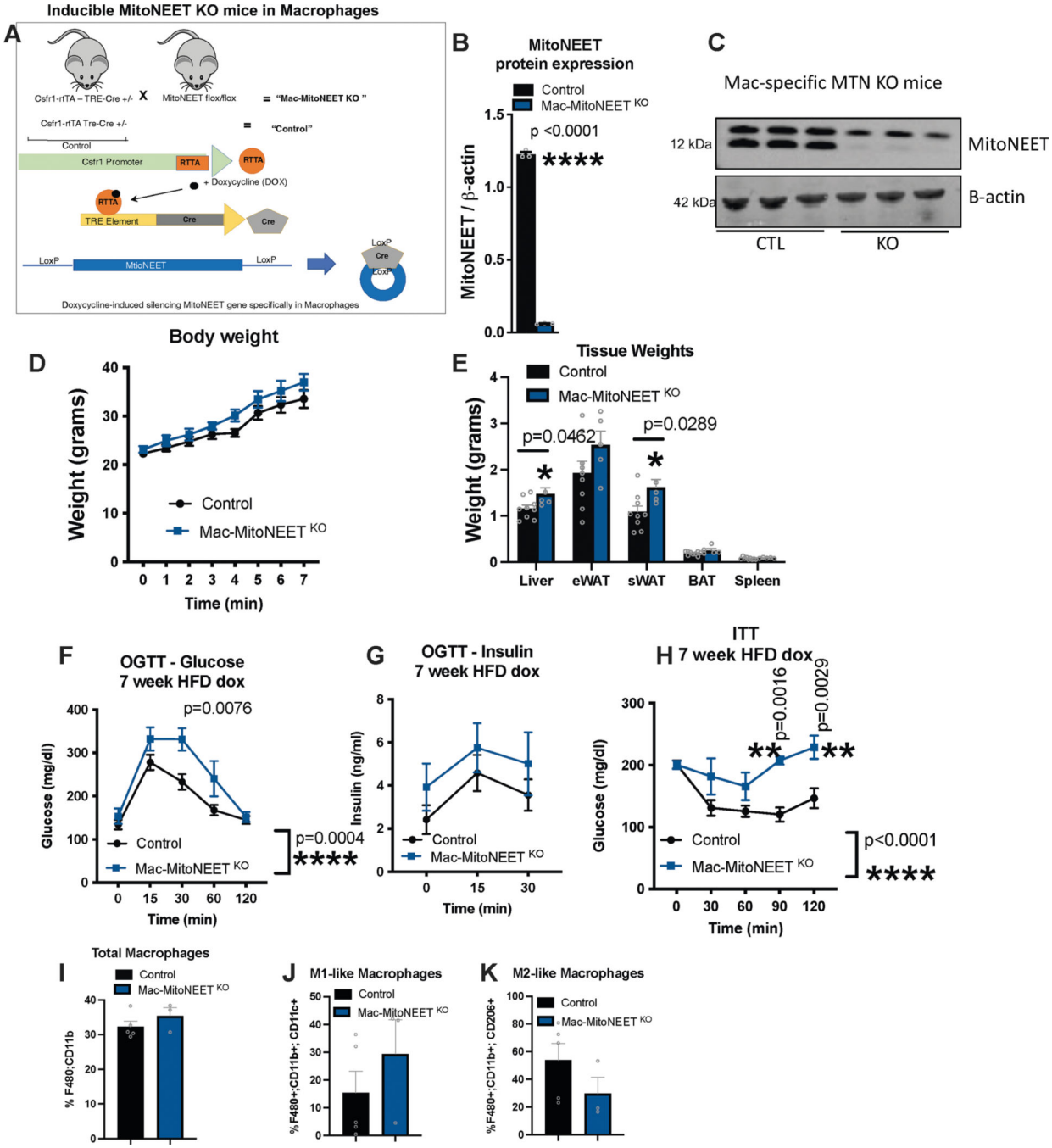

Extended Data Fig. 7 |. Eliminating MitoNEET in macrophages during HFD promotes insulin resistance and inflammation.

(a-k) Six-week-old male control and Mac-MitoNEET^{KO} mice were fed HFD dox for 7 weeks. **(a)** Breeding strategy. **(b)** MitoNEET protein expression relative to β-actin in peritoneal macrophages (n = 3). **(c)** Representative Western blots (n = 3). **(d)** Body weight (control n = 9, TG n = 5). **(e)** Tissue weights (control n = 9, TG n = 5). **(f-g)** Oral glucose tolerance test. **(f)** Blood glucose levels (control n = 5, TG n = 3). **(g)** Serum insulin levels (control n = 9, TG n = 5). **(h)** Blood glucose levels during insulin tolerance test

(control n = 9, TG n = 5). **(i-k)** Flow cytometric measurement of total, M1-like and M2-like macrophages in eWAT (control n = 5, TG n = 3). Significance in **(b, e, i-k)** between control and Mac-MitoNEET^{KO} was calculated using a two-tailed Student's t-test. Significance in **(d, f-h)** was calculated using a 2-way ANOVA with Sidak's post-test for multiple comparisons. Error bars represent mean ± S.E.M. * (P < 0.05), ** (p < 0.01), *** (p < 0.0001), **** (p < 0.00001).

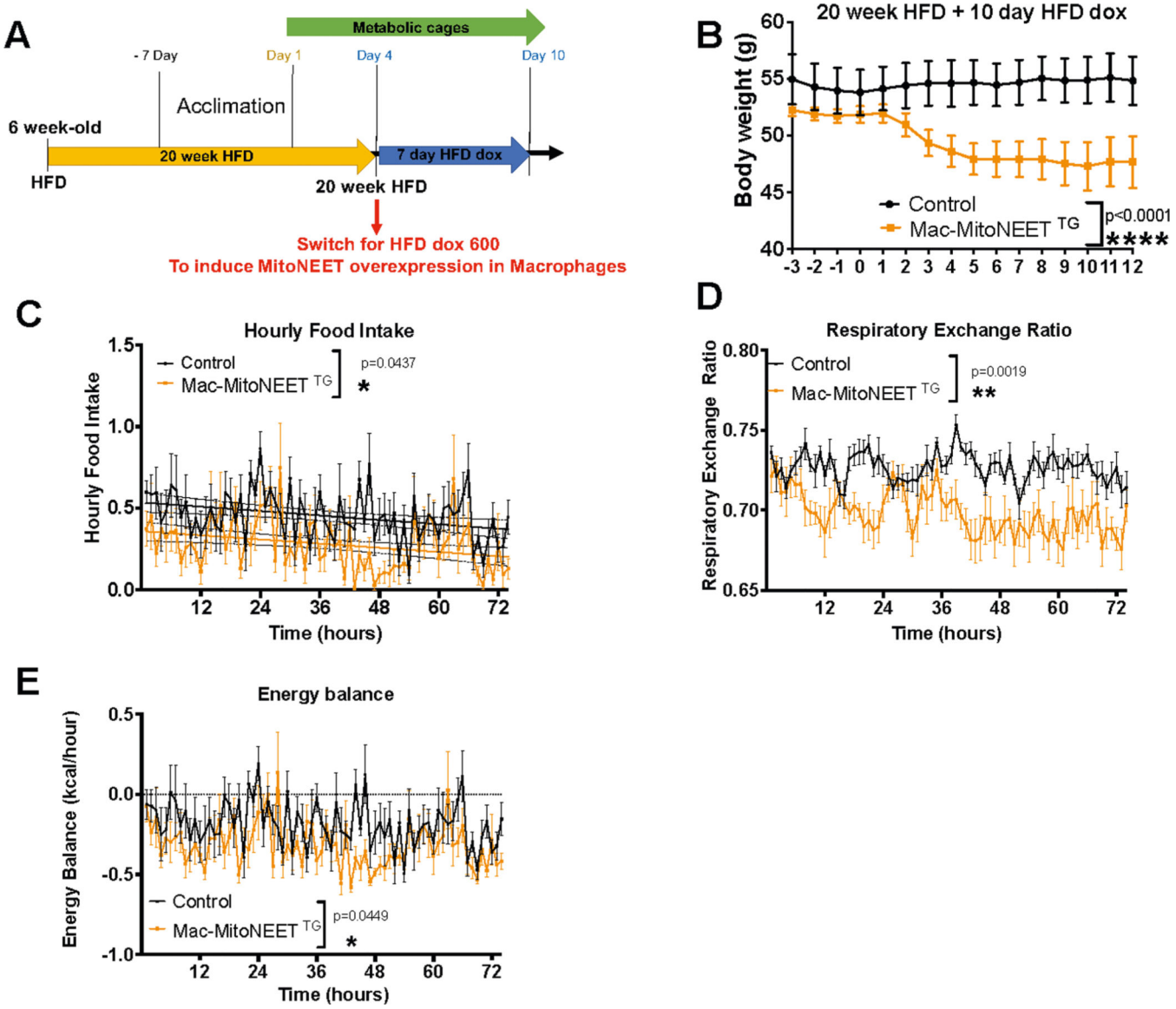

Extended Data Fig. 8 |. Metabolic analyses of Mac-MitoNEET^{TG} mice.

(a-e) Six-week-old male control and Mac-MitoNEET^{TG} mice were fed HFD for 20 weeks and then switched to HFD dox for 1 week. Metabolic analyses were performed at 3 d before and 7 d after diet change (n = 6). **(a)** Experimental design. **(b)** Body weight (n = 5). **(c)** Hourly food intake (n = 6). **(d)** Respiratory exchange ratio (n = 6). **(e)** Energy balance (n = 6). Significance in **(b-e)** between control and Mac-MitoNEET^{TG} was calculated using a

2-way ANOVA with Sidak's post-test for multiple comparisons. Error bars represent mean ± S.E.M. * (P < 0.05), ** (p < 0.01), *** (p < 0.0001), **** (p < 0.00001).

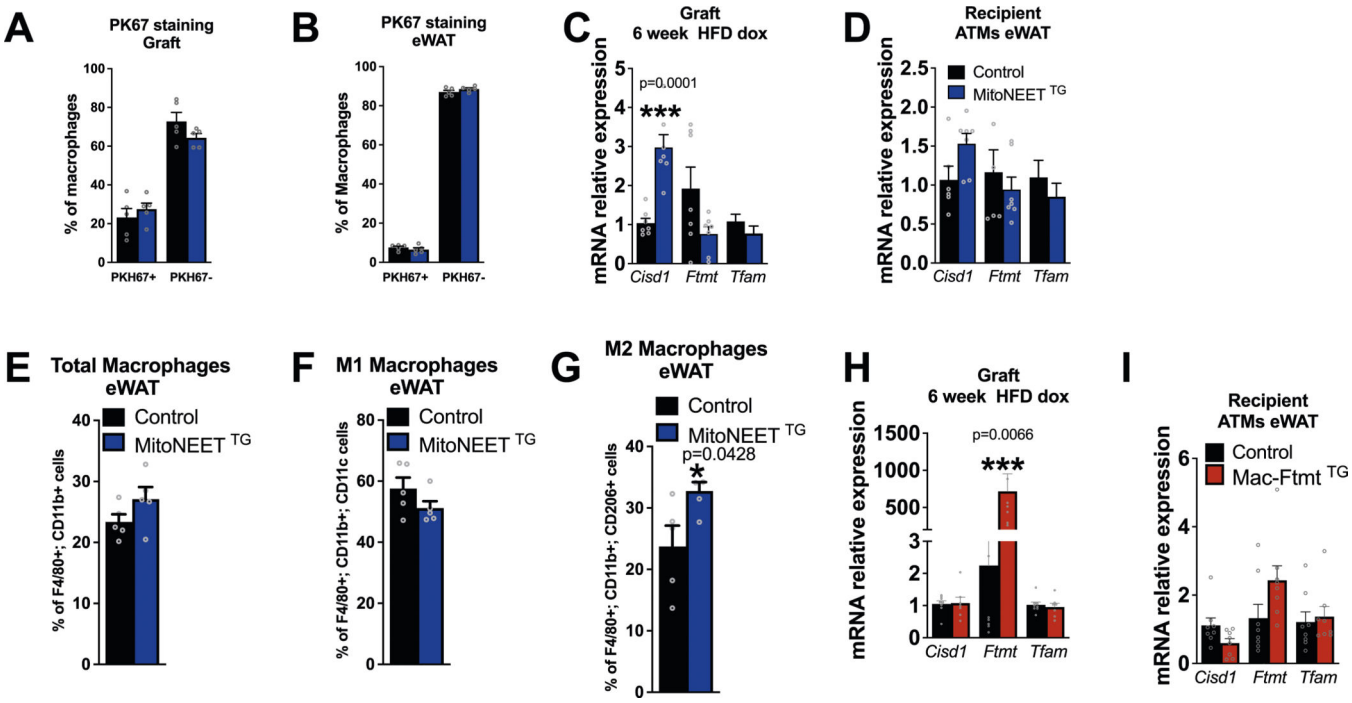

Extended Data Fig. 9 |. Validation of eWAT transplantation to wild-type mice.

(a-i) Six-week-old male control and Mac-MitoNEET^{TG} mice were injected with PKH67 dye before transplantation of their eWAT to wild-type mice (n = 5). Recipient mice were allowed to recover 3 weeks and then fed HFD dox for 6 weeks. **(a-b)** Flow cytometric measurement of PKH67 fluorescence in **(a)** graft and **(b)** recipient eWAT (n = 5). **(c-d)** mRNA levels of *Cisd1*, *Ftmt*, and *Tfam* relative to control in **(c)** graft and **(d)** recipient eWAT (n = 5). **(e-g)** Flow cytometric measurement of total, M1-like, and M2-like macrophages in recipient eWAT (n = 5). **(h-i)** Wild-type mice were transplanted with either control or Mac-Ftmt^{TG} eWAT. Transplanted mice were allowed to recover 3 weeks and then fed HFD dox for 6 weeks. **(h-i)** mRNA levels of *Cisd1*, *Ftmt* and *Tfam* relative to control in **(c)** graft and **(d)** recipient eWAT (control n = 7, TG n = 8). Significance in **(a-i)** between control and transgenic fat-transplanted animals was calculated using a two-tailed Student's t-test. Error bars represent mean ± S.E.M. * (P < 0.05), ** (p < 0.01), *** (p < 0.0001), **** (p < 0.00001).

Supplementary Material

Refer to Web version on PubMed Central for supplementary material.

Acknowledgements

We thank the UTSW Animal Resource Center, Histology Core, Metabolic Phenotyping Core, the Live Cell Imaging Core, Transgenic Core and Flow Cytometry Facility for their excellent assistance with experiments performed in this paper. We also thank Shimadzu Scientific Instruments for the collaborative efforts in mass spectrometry technology resources. This study was supported by US National Institute of Health grants RC2-DK118620, R01-

DK55758, R01-DK099110, R01-DK127274 and R01-DK131537 to P.E.S.; R01 DK108773 to D.Y.O.; C.C. is supported by K99-DK122019 and R00-DK122019. C.M.G. is supported by F32-DK-122623; V.A.P. was supported by an American Diabetes Association Minority Postdoctoral Fellowship (1-18-PMF-030). J.-B.F. was supported by the Deutsche Forschungsgemeinschaft (DFG, German Research Foundation; grant 414232833).

Data availability

All data generated or analysed during this study are available with this paper. Source data are provided with this paper.

References

1. Gustafson B, Hedjazifar S, Gogg S, Hammarstedt A. & Smith U. Insulin resistance and impaired adipogenesis. Trends Endocrinol. Metab. 26, 193–200 (2015). [PubMed: 25703677]
2. Kloting N. & Bluher M. Adipocyte dysfunction, inflammation and metabolic syndrome. Rev. Endocr. Metab. Disord 15, 277–287 (2014). [PubMed: 25344447]
3. Sun K, Kusminski CM & Scherer PE Adipose tissue remodeling and obesity. J. Clin. Invest 121, 2094–2101 (2011). [PubMed: 21633177]
4. Sun K, Tordjman J, Clement K. & Scherer PE Fibrosis and adipose tissue dysfunction. Cell Metab. 18, 470–477 (2013). [PubMed: 23954640]
5. Chaurasia B. & Summers SA Ceramides—lipotoxic inducers of metabolic disorders: (Trends in Endocrinology and Metabolism 26, 538–550; 2015). Trends Endocrinol. Metab 29, 66–67 (2018). [PubMed: 28988873]
6. Perry RJ, Samuel VT, Petersen KF & Shulman GI The role of hepatic lipids in hepatic insulin resistance and type 2 diabetes. Nature 510, 84–91 (2014). [PubMed: 24899308]
7. Kusminski CM, Shetty S, Orci L, Unger RH & Scherer PE Diabetes and apoptosis: lipotoxicity. Apoptosis 14, 1484–1495 (2009). [PubMed: 19421860]
8. Winer S. & Winer DA The adaptive immune system as a fundamental regulator of adipose tissue inflammation and insulin resistance. Immunol. Cell Biol 90, 755–762 (2012). [PubMed: 22231651]
9. Weisberg SP et al. Obesity is associated with macrophage accumulation in adipose tissue. J. Clin. Invest 112, 1796–1808 (2003). [PubMed: 14679176]
10. Lumeng CN, Bodzin JL & Saltiel AR Obesity induces a phenotypic switch in adipose tissue macrophage polarization. J. Clin. Invest 117, 175–184 (2007). [PubMed: 17200717]
11. Orr JS et al. Obesity alters adipose tissue macrophage iron content and tissue iron distribution. Diabetes 63, 421–432 (2014). [PubMed: 24130337]
12. Hubler MJ, Erikson KM, Kennedy AJ & Hasty AH MFe^{hi} adipose tissue macrophages compensate for tissue iron perturbations in mice. Am. J. Physiol. Cell Physiol 315, C319–C329 (2018). [PubMed: 29768045]
13. Joffin N. et al. Mitochondrial metabolism is a key regulator of the fibro-inflammatory and adipogenic stromal subpopulations in white adipose tissue. Cell Stem Cell 10.1016/j.stem.2021.01.002 (2021).
14. Zhang Z. et al. Adipocyte iron levels impinge on a fat-gut cross-talk to regulate intestinal lipid absorption and mediate protection from obesity. Cell Metab. 33, 1624–1639 (2021). [PubMed: 34174197]
15. Ameka MK & Hasty AH Fat and iron don't mix. Immunometabolism 10.20900/immunometab20200034 (2020).
16. Gabrielsen JS et al. Adipocyte iron regulates adiponectin and insulin sensitivity. J. Clin. Invest 122, 3529–3540 (2012). [PubMed: 22996660]
17. Zheng J, Chen M, Liu G, Xu E. & Chen H. Ablation of hephaestin and ceruloplasmin results in iron accumulation in adipocytes and type 2 diabetes. FEBS Lett. 592, 394–401 (2018). [PubMed: 29355933]
18. Mills EL & O'Neill LA Reprogramming mitochondrial metabolism in macrophages as an anti-inflammatory signal. Eur. J. Immunol 46, 13–21 (2016). [PubMed: 26643360]

19. Van den Bossche J. et al. Mitochondrial dysfunction prevents repolarization of inflammatory macrophages. Cell Rep. 17, 684–696 (2016). [PubMed: 27732846]
20. Aerbajinai W. et al. Glia maturation factor-gamma regulates murine macrophage iron metabolism and M2 polarization through mitochondrial ROS. Blood Adv. 3, 1211–1225 (2019). [PubMed: 30971398]
21. Drapier JC & Hibbs JB Jr. Differentiation of murine macrophages to express nonspecific cytotoxicity for tumor cells results in L-arginine-dependent inhibition of mitochondrial iron-sulfur enzymes in the macrophage effector cells. J. Immunol 140, 2829–2838 (1988). [PubMed: 2451695]
22. Soares MP & Hamza I. Macrophages and iron metabolism. Immunity 44, 492–504 (2016). [PubMed: 26982356]
23. Tong WH et al. TLR-activated repression of Fe–S cluster biogenesis drives a metabolic shift and alters histone and tubulin acetylation. Blood Adv. 2, 1146–1156 (2018). [PubMed: 29784770]
24. Barros MH, Hauck F, Dreyer JH, Kempkes B. & Niedobitek G. Macrophage polarisation: an immunohistochemical approach for identifying M1 and M2 macrophages. PLoS ONE 8, e80908 (2013). [PubMed: 24260507]
25. Moreno-Navarrete JM et al. HMOX1 as a marker of iron excess-induced adipose tissue dysfunction, affecting glucose uptake and respiratory capacity in human adipocytes. Diabetologia 60, 915–926 (2017). [PubMed: 28243792]
26. Lee W, Yun S, Choi GH & Jung TW Fibronectin type III domain containing 4 attenuates hyperlipidemia-induced insulin resistance via suppression of inflammation and ER stress through HO-1 expression in adipocytes. Biochem. Biophys. Res. Commun 502, 129–136 (2018). [PubMed: 29787756]
27. Kusminski CM et al. MitoNEET-driven alterations in adipocyte mitochondrial activity reveal a crucial adaptive process that preserves insulin sensitivity in obesity. Nat. Med 18, 1539–1549 (2012). [PubMed: 22961109]
28. Kusminski CM, Park J. & Scherer PE MitoNEET-mediated effects on browning of white adipose tissue. Nat. Commun 5, 3962 (2014). [PubMed: 24865177]
29. Corsi B. et al. Human mitochondrial ferritin expressed in HeLa cells incorporates iron and affects cellular iron metabolism. J. Biol. Chem 277, 22430–22437 (2002). [PubMed: 11953424]
30. Kusminski CM et al. A novel model of diabetic complications: adipocyte mitochondrial dysfunction triggers massive beta-cell hyperplasia. Diabetes 69, 313–330 (2020). [PubMed: 31882562]
31. Zhu Q. et al. Suppressing adipocyte inflammation promotes insulin resistance in mice. Mol. Metab 39, 101010 (2020).
32. Fernandez-Real JM, Lopez-Bermejo A. & Ricart W. Cross-talk between iron metabolism and diabetes. Diabetes 51, 2348–2354 (2002). [PubMed: 12145144]
33. Ford ES & Cogswell ME Diabetes and serum ferritin concentration among US adults. Diabetes Care 22, 1978–1983 (1999). [PubMed: 10587829]
34. Jiang R. et al. Body iron stores in relation to risk of type 2 diabetes in apparently healthy women. JAMA 291, 711–717 (2004). [PubMed: 14871914]
35. Forouhi NG et al. Elevated serum ferritin levels predict new-onset type 2 diabetes: results from the EPIC-Norfolk prospective study. Diabetologia 50, 949–956 (2007). [PubMed: 17333112]
36. Corna G. et al. Polarization dictates iron handling by inflammatory and alternatively activated macrophages. Haematologica 95, 1814–1822 (2010). [PubMed: 20511666]
37. Recalcati S. et al. Differential regulation of iron homeostasis during human macrophage polarized activation. Eur. J. Immunol 40, 824–835 (2010). [PubMed: 20039303]
38. Hubler MJ, Peterson KR & Hasty AH Iron homeostasis: a new job for macrophages in adipose tissue? Trends Endocrinol. Metab 26, 101–109 (2015). [PubMed: 25600948]
39. de Mello AH, Costa AB, Engel JDG & Rezin GT Mitochondrial dysfunction in obesity. Life Sci. 192, 26–32 (2018). [PubMed: 29155300]
40. Caslin HL, Bhanot M, Bolus WR & Hasty AH Adipose tissue macrophages: unique polarization and bioenergetics in obesity. Immunol. Rev 295, 101–113 (2020). [PubMed: 32237081]

41. Rodriguez-Prados JC et al. Substrate fate in activated macrophages: a comparison between innate, classic, and alternative activation. J. Immunol 185, 605–614 (2010). [PubMed: 20498354]
42. Pereira M. et al. Acute iron deprivation reprograms human macrophage metabolism and reduces inflammation in vivo. Cell Rep. 28, 498–511 (2019). [PubMed: 31291584]
43. Tannahill GM et al. Succinate is an inflammatory signal that induces IL-1β through HIF-1α. Nature 496, 238–242 (2013). [PubMed: 23535595]
44. Jha AK et al. Network integration of parallel metabolic and transcriptional data reveals metabolic modules that regulate macrophage polarization. Immunity 42, 419–430 (2015). [PubMed: 25786174]
45. El Kasmi KC & Stenmark KR Contribution of metabolic reprogramming to macrophage plasticity and function. Semin. Immunol 27, 267–275 (2015). [PubMed: 26454572]
46. Galvan-Pena S. & O'Neill LA Metabolic reprograming in macrophage polarization. Front Immunol. 5, 420 (2014). [PubMed: 25228902]
47. Crooks DR et al. Acute loss of iron-sulfur clusters results in metabolic reprogramming and generation of lipid droplets in mammalian cells. J. Biol. Chem 293, 8297–8311 (2018). [PubMed: 29523684]
48. Behmoaras J. The versatile biochemistry of iron in macrophage effector functions. FEBS J. 288, 6972–6989 (2021). [PubMed: 33354925]
49. Kelly B. & O'Neill LA Metabolic reprogramming in macrophages and dendritic cells in innate immunity. Cell Res. 25, 771–784 (2015). [PubMed: 26045163]
50. Palsson-McDermott EM et al. Pyruvate kinase M2 regulates Hif-1α activity and IL-1β induction and is a critical determinant of the warburg effect in LPS-activated macrophages. Cell Metab. 21, 65–80 (2015). [PubMed: 25565206]
51. Mounier R. et al. AMPKα1 regulates macrophage skewing at the time of resolution of inflammation during skeletal muscle regeneration. Cell Metab. 18, 251–264 (2013). [PubMed: 23931756]
52. Shapiro H, Lutaty A. & Ariel A. Macrophages, meta-inflammation, and immuno-metabolism. ScientificWorldJournal 11, 2509–2529 (2011). [PubMed: 22235182]
53. Angajala A. et al. Diverse roles of mitochondria in immune responses: novel insights into immuno-metabolism. Front Immunol. 9, 1605 (2018). [PubMed: 30050539]
54. Wang H, Liu C, Zhao Y. & Gao G. Mitochondria regulation in ferroptosis. Eur. J. Cell Biol 99, 151058 (2020).
55. Sumneang N, Siri-Angkul N, Kumfu S, Chattipakorn SC & Chattipakorn N. The effects of iron overload on mitochondrial function, mitochondrial dynamics, and ferroptosis in cardiomyocytes. Arch. Biochem. Biophys 680, 108241 (2020).
56. Tajima S. et al. Iron reduction by deferoxamine leads to amelioration of adiposity via the regulation of oxidative stress and inflammation in obese and type 2 diabetes KKAy mice. Am. J. Physiol. Endocrinol. Metab 302, E77–E86 (2012). [PubMed: 21917632]
57. Green A, Basile R. & Rumberger JM Transferrin and iron induce insulin resistance of glucose transport in adipocytes. Metabolism 55, 1042–1045 (2006). [PubMed: 16839839]
58. Cooksey RC et al. Dietary iron restriction or iron chelation protects from diabetes and loss of beta-cell function in the obese (ob/ob lep−/−) mouse. Am. J. Physiol. Endocrinol. Metab 298, E1236–E1243 (2010). [PubMed: 20354157]
59. Minamiyama Y. et al. Iron restriction improves type 2 diabetes mellitus in Otsuka Long-Evans Tokushima fatty rats. Am. J. Physiol. Endocrinol. Metab 298, E1140–E1149 (2010). [PubMed: 20215574]
60. Valenti L. et al. Iron depletion by phlebotomy improves insulin resistance in patients with nonalcoholic fatty liver disease and hyperferritinemia: evidence from a case–control study. Am. J. Gastroenterol 102, 1251–1258 (2007). [PubMed: 17391316]
61. Valenti L. et al. Venesection for non-alcoholic fatty liver disease unresponsive to lifestyle counselling—a propensity score-adjusted observational study. QJM 104, 141–149 (2011). [PubMed: 20851820]
62. Gao Y. et al. Adipocyte iron regulates leptin and food intake. J. Clin. Invest 125, 3681–3691 (2015). [PubMed: 26301810]

63. Tomay F. et al. Purple corn extract induces long-lasting reprogramming and M2 phenotypic switch of adipose tissue macrophages in obese mice. J. Transl. Med 17, 237 (2019). [PubMed: 31337415]

64. Weiss G, Bogdan C. & Hentze MW Pathways for the regulation of macrophage iron metabolism by the anti-inflammatory cytokines IL-4 and IL-13. J. Immunol 158, 420–425 (1997). [PubMed: 8977218]

65. Brock JH, Djeha A, Ismail M, Oria R. & Sinclair RH Cellular responses to iron and iron compounds. Adv. Exp. Med Biol 356, 91–100 (1994). [PubMed: 7887249]

66. Weiss G. et al. Iron modulates interferon-gamma effects in the human myelomonocytic cell line THP-1. Exp. Hematol 20, 605–610 (1992). [PubMed: 1587306]

67. Sugimoto M. et al. MMMDB: Mouse Multiple Tissue Metabolome Database. Nucleic Acids Res. 40, D809–D814 (2012). [PubMed: 22139941]

68. Fraenkel PG Anemia of inflammation: a review. Med. Clin. North Am 101, 285–296 (2017). [PubMed: 28189171]

69. Livak KJ & Schmittgen TD Analysis of relative gene expression data using real-time quantitative PCR and the $2^{-\Delta\Delta CT}$ method. Methods 25, 402–408 (2001). [PubMed: 11846609]

70. Peics J. et al. Isolation of adipogenic and fibro-inflammatory stromal cell subpopulations from murine intra-abdominal adipose depots. J. Vis. Exp 10.3791/61610 (2020).

71. Pinero DJ, Li N, Hu J, Beard JL & Connor JR The intracellular location of iron regulatory proteins is altered as a function of iron status in cell cultures and rat brain. J. Nutr 131, 2831–2836 (2001). [PubMed: 11694604]

72. Gao Y. et al. Iron downregulates leptin by suppressing protein O-GlcNAc modification in adipocytes, resulting in decreased levels of O-glycosylated CREB. J. Biol. Chem 294, 5487–5495 (2019). [PubMed: 30709903]

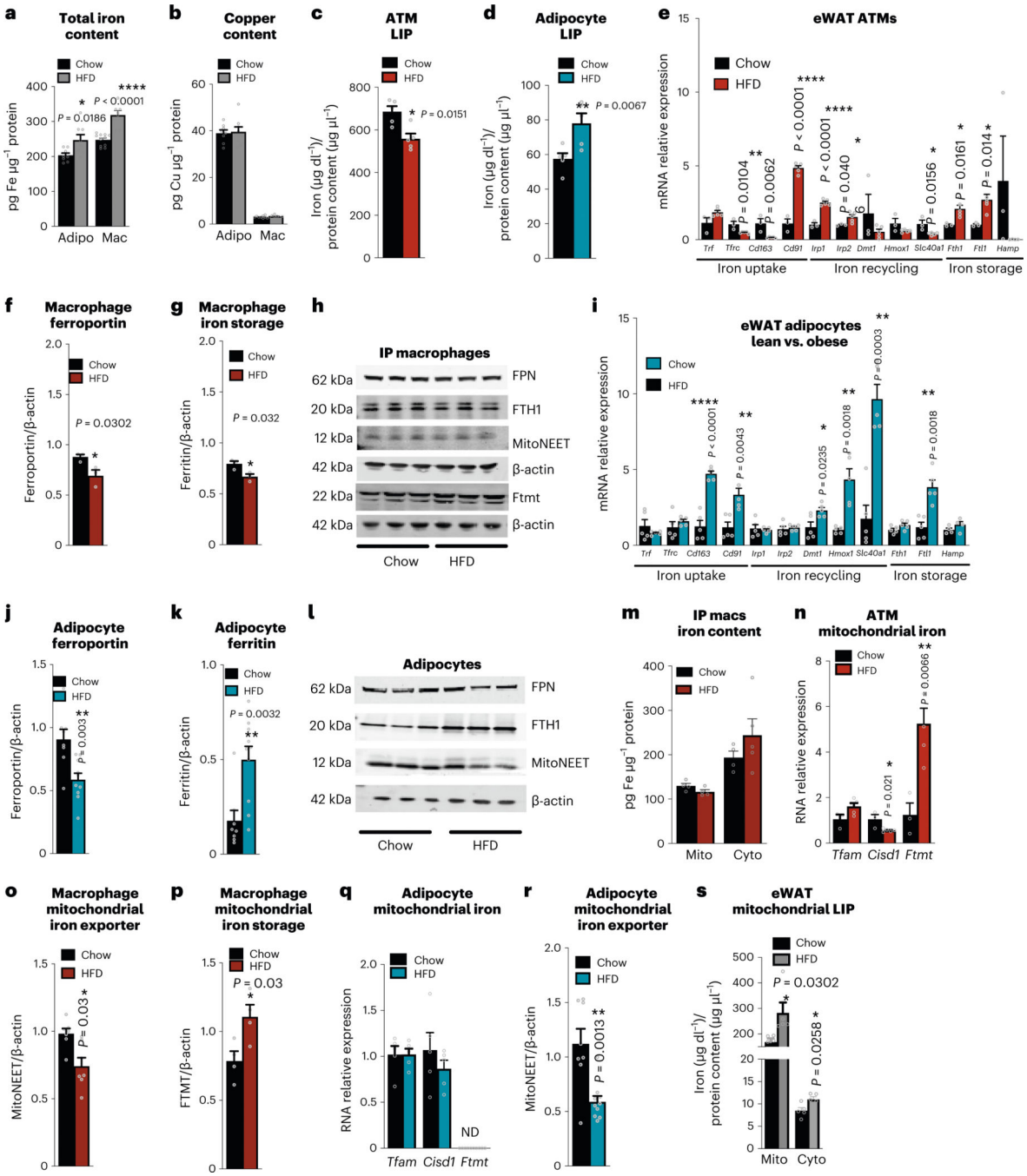

Fig. 1 |. Obesity leads to mitochondrial iron overload in adipose tissue macrophages.

a–**s**, Six-week-old male wild-type mice were fed either normal chow diet or HFD for 10 weeks. **a**, Total iron content measured by ICP-MS in adipocytes and peritoneal macrophages (chow $n = 8$, HFD $n = 12$). **b**, Total copper content measured by ICP-MS in adipocytes and ATMs from eWAT (chow $n = 8$, HFD $n = 12$). **c**,**d**, LIP in ATMs ($n = 5$; **c**) and adipocytes ($n = 5$; **d**) from eWAT. **e**, mRNA levels of iron metabolism genes relative to chow in ATMs from eWAT (chow $n = 3$, HFD $n = 5$). **f**,**g**, Ferroportin (**f**) and ferritin (**g**) protein expression relative to β-actin in peritoneal MACs ($n = 3$). **h**, Representative western blots chosen from

three independent experiments. **i**, mRNA levels of iron metabolism genes relative to chow in adipocytes from eWAT ($n = 5$). **j**,**k**, Ferroportin (**j**) and ferritin (**k**) protein expression relative to β-actin in adipocytes from eWAT (chow $n = 8$, HFD $n = 10$). **l**, Representative western blots chosen from eight independent experiments. **m**, Total iron content measured by ICP-MS in mitochondrial ($n = 4$) and cytosolic compartments of ATMs from eWAT (chow $n = 4$, HFD $n = 5$). **n**, mRNA levels of mitochondrial iron metabolism genes relative to chow in ATMs from eWAT (chow $n = 3$, HFD $n = 5$). **o**,**p**, MitoNEET ($n = 7$; **o**) and FTMT ($n = 4$; **p**) protein expression relative to β-actin in ATMs from eWAT. **q**, mRNA levels of mitochondrial iron metabolism genes relative to lean in adipocytes from eWAT ($n = 5$). **r**, MitoNEET protein expression relative to β-actin in adipocytes from eWAT (chow $n = 8$, HFD $n = 10$). **s**, LIP in in mitochondrial and cytosolic compartments of eWAT ($n = 5$). Significance between chow and HFD was calculated using a two-tailed Student's *t*-test. Error bars represent the mean ± s.e.m. $*P < 0.05$, $**P < 0.01$, $P < 0.001$, $****P < 0.0001$. IP mac, peritoneal macrophage; ND, not determined.

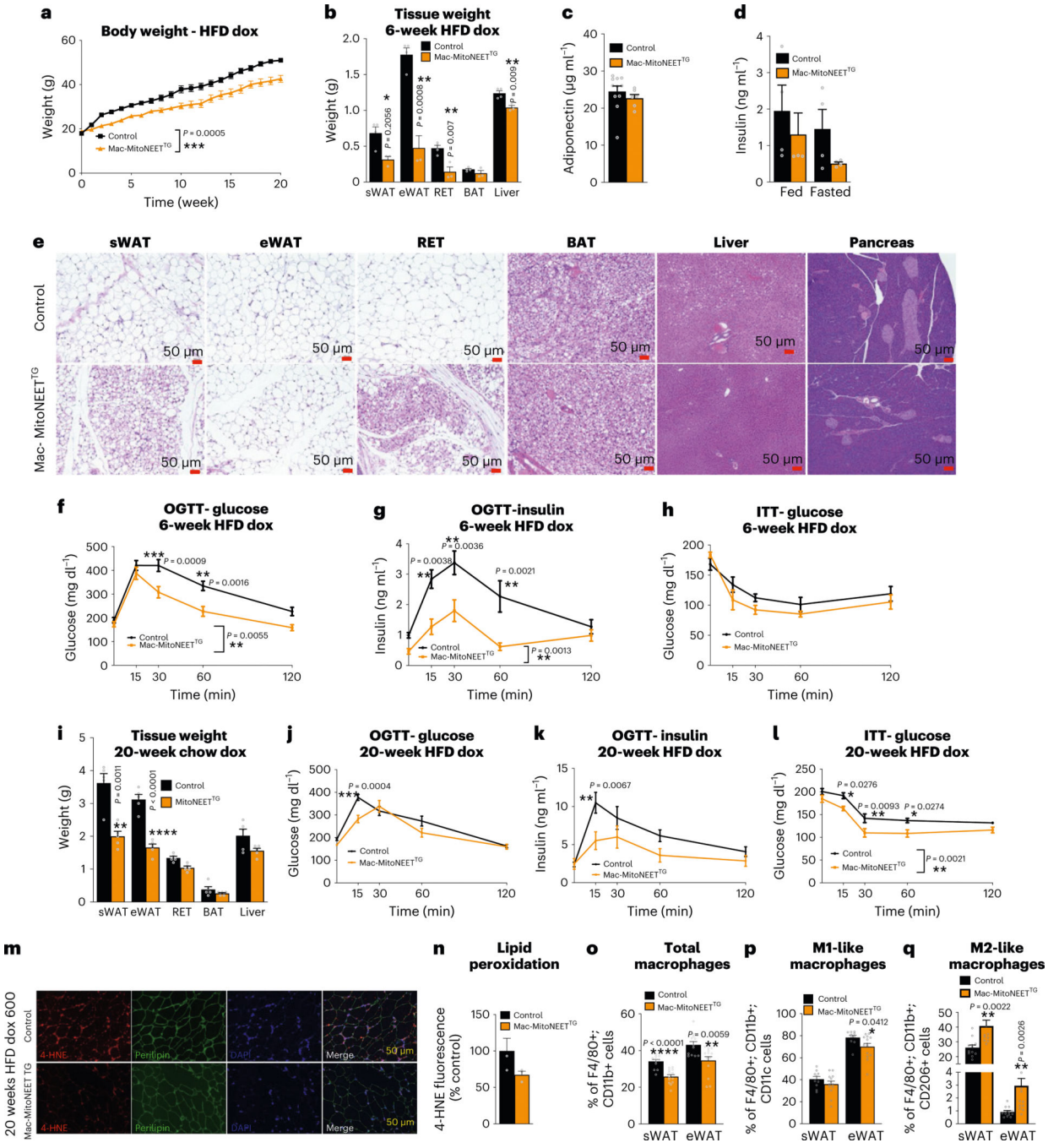

Fig. 2 |. Mac-MitoNEET^{TG} mice are protected from HFD-induced obesity and metabolic disorders.

a, Six-week-old male control and Mac-MitoNEET^{TG} mice were fed HFD dox for 20 weeks. **a**, Body weight (control $n = 21$, TG $n = 22$). **b**–**h**, Data after 6 weeks of HFD dox feeding. **b**, Tissue weights (control $n = 4$, TG $n = 3$). **c**, Serum adiponectin levels (control $n = 11$, TG $n = 6$). **d**, Serum insulin levels in the fed and fasted states ($n = 4$). Tissue histology with haematoxylin and eosin (H&E) staining chosen from three independent experiments. **f**,**g**, Oral glucose tolerance test (OGTT). **f**, Serum glucose levels (control $n = 12$, TG $n = 8$).

g, Serum insulin levels (control $n = 10$, TG $n = 7$). **h**, Insulin tolerance test (ITT; control $n = 7$, TG $n = 4$). **i**–**q**, Data after 20 weeks of HFD dox feeding. **i**, Tissue weights ($n = 5$). **j**,**k**, Oral glucose tolerance test. **j**, Serum glucose levels (control $n = 12$, TG $n = 8$). **k**, Serum insulin levels (control $n = 8$, TG $n = 6$). **l**, Insulin tolerance test (control $n = 7$, TG $n = 9$). **m**, Representative fluorescence micrographs of 4-HNE, perilipin and DAPI staining of eWAT chosen from three independent experiments. **n**, Quantification of 4-HNE fluorescence signal relative to control ($n = 3$). **o**–**q**, Flow cytometric measurement from sWAT and eWAT of total macrophages (sWAT control $n = 12$, TG $n = 13$; eWAT control $n = 12$, TG $n = 13$), M1-like macrophages (sWAT control $n = 10$, TG $n = 13$; eWAT control $n = 10$, TG $n = 14$) and M2-like macrophages (sWAT control $n = 12$, TG $n = 11$; eWAT control $n = 12$, TG $n = 14$). Significance in **a**, **f**–**h** and **j**–**l** between control and Mac-MitoNEET^{TG} was calculated using a two-way analysis of variance (ANOVA) with Sidak's post hoc test for multiple comparisons. Significance in **b**–**d**, **i** and **n**–**q** between control and Mac-MitoNEET^{TG} was calculated using a two-tailed Student's *t*-test. Error bars represent the mean ± s.e.m. *$P < 0.05$), **$P < 0.01$, ***$P < 0.001$, ****$P < 0.0001$.

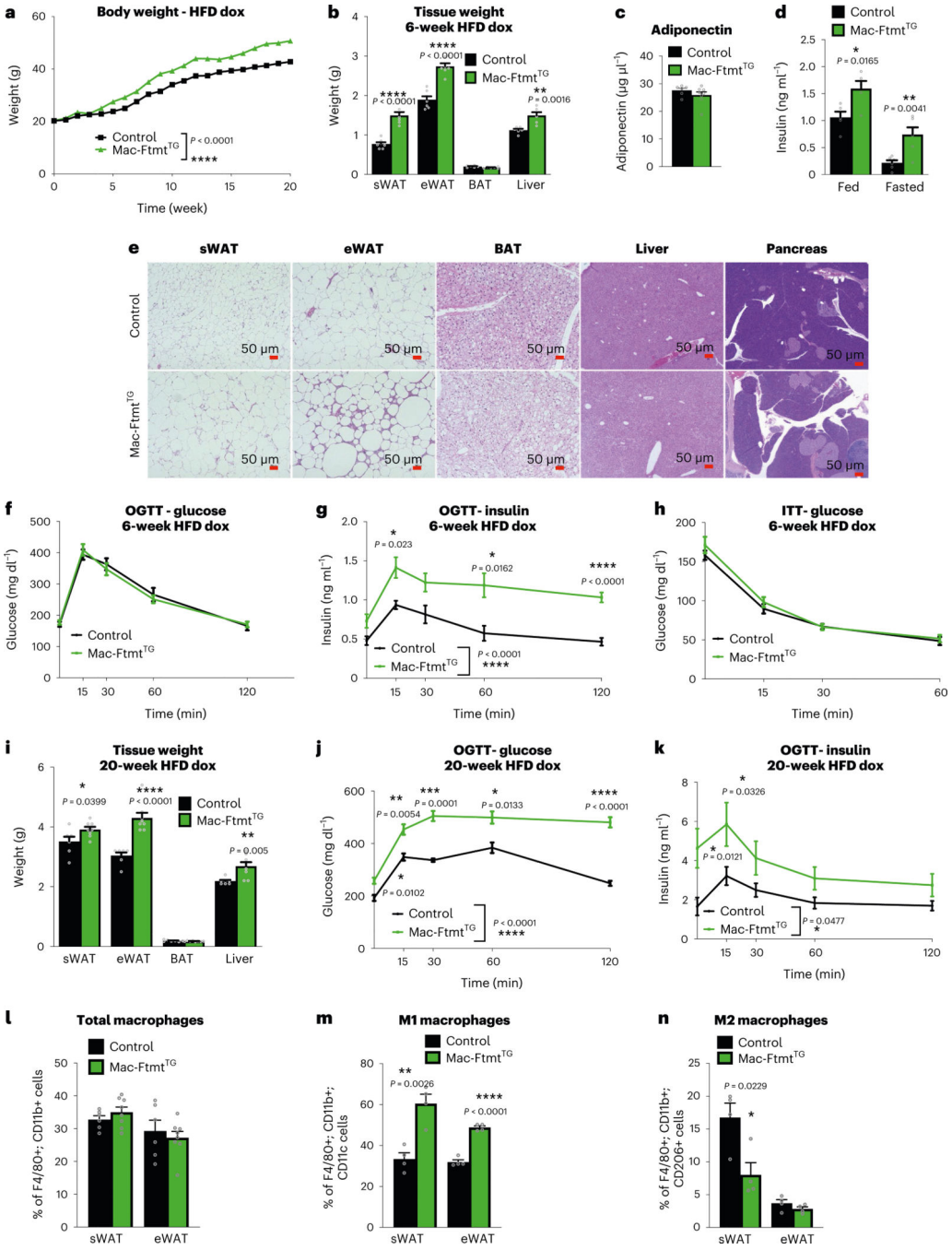

Fig. 3 |. Mac-Ftmt^{TG} mice are more susceptible to high-fat-diet-induced obesity and metabolic disorders.

a, Six-week-old male control and Mac-Ftmt^{TG} mice were fed HFD + dox for 20 weeks. **a**, Body weight (control $n = 7$, TG $n = 8$). **b**–**h**, Data after 6 weeks of HFD dox feeding. **b**, Tissue weights (sWAT and eWAT, $n = 7$; retroperitoneal white adipose tissue (RET), BAT and liver, $n = 6$). **c**, Serum adiponectin levels (control $n = 6$, TG = 8). **d**, Serum insulin levels in the fed state ($n = 5$) and fasted state ($n = 6$). **e**, Tissue histology with H&E staining chosen from three independent experiments. **f**,**g**, Oral glucose tolerance test. **f**, Serum glucose levels

(n = 13). **g**, Serum insulin levels (n = 12). **h**, Insulin tolerance test (n = 13). **i**–**n**, Data after 20 weeks of HFD dox feeding. **i**, Tissue weights (control n = 7, TG = 8). **j**,**k**, Oral glucose tolerance test. **j**, Serum glucose levels (control n = 6, TG n = 8). **k**, Serum insulin levels (n = 6). **l**–**n**, Flow cytometric measurements from sWAT and eWAT of total macrophages (control n = 6, TG n = 8), M1-like (n = 4) and M2-like (n = 4) macrophages. Significance in **a**, **f**–**h** and **j** and **k** between control and Mac-Ftmt^{TG} was calculated using a two-way ANOVA with Sidak's post hoc test for multiple comparisons. Significance in **b**–**d**, **i** and **l**–**n** between control and Mac-Ftmt^{TG} was calculated using a two-tailed Student's t-test. Error bars represent the mean ± s.e.m. *P < 0.05, **P < 0.01, ***P < 0.001, ****P < 0.0001.

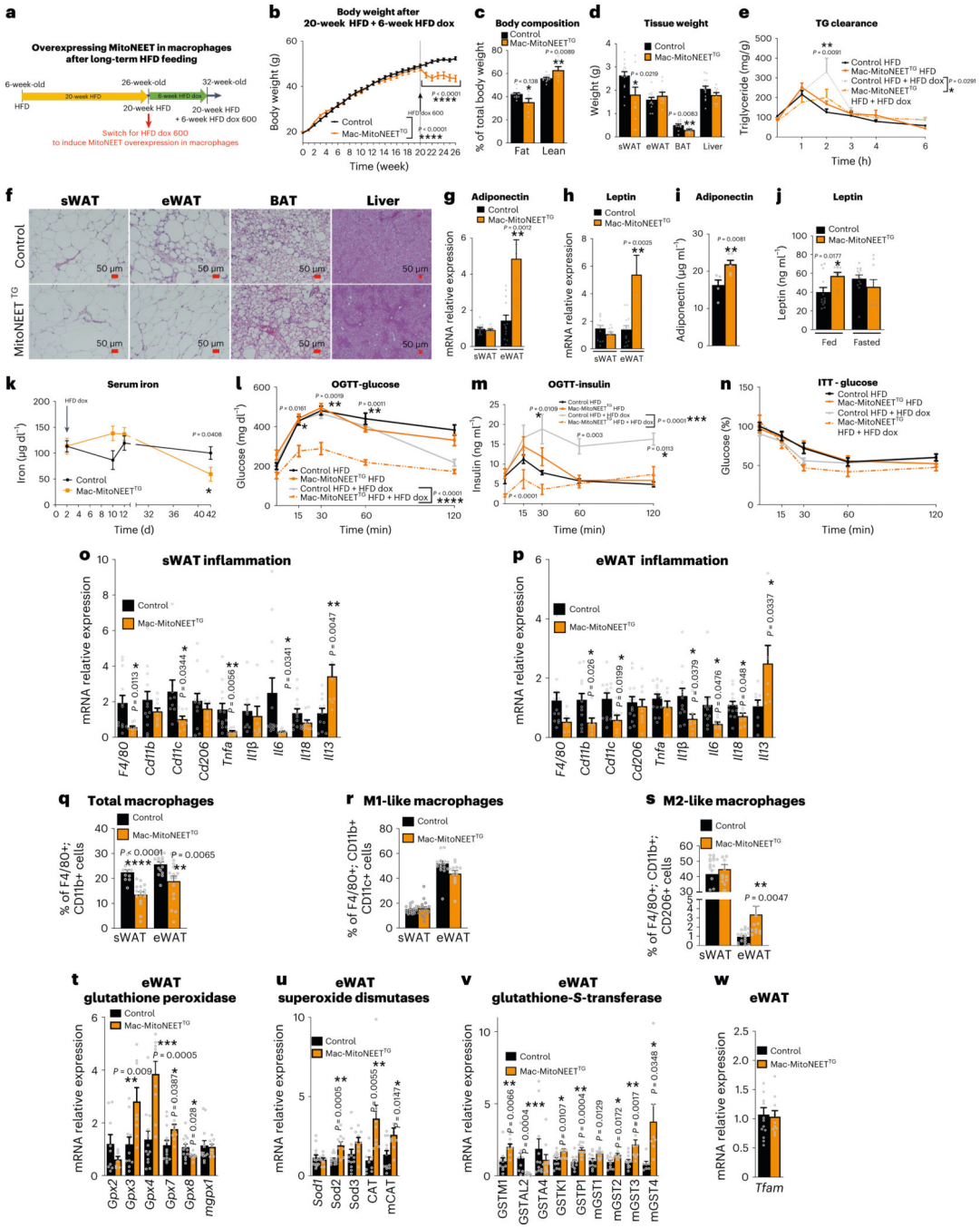

Fig. 4 |. Reducing mitochondrial iron content in macrophages after a long-term high-fat-diet feeding reverses obesity and metabolic dysfunction.

a–**w**, Male control and Mac-MitoNEET^{TG} mice were fed a HFD for 20 weeks and then switched to HFD dox for an additional 6 weeks. **a**, Experimental design. **b**, Body weight (control $n = 19$, TG $n = 21$). **c**, Body composition (control $n = 13$, TG $n = 7$). **d**, Tissue weights (sWAT and liver control $n = 14$, TG = 10, BAT control $n = 13$, TG $n = 9$, eWAT control $n = 14$, TG $n = 9$). **e**, Triglyceride (TG) clearance (HFD: control $n = 18$, TG $n = 13$; HFD dox: control $n = 12$, TG $n = 10$). **f**, Tissue histology with H&E staining. **g**,**h**,

Adiponectin (**g**) and leptin (**h**) mRNA levels relative to control in sWAT and eWAT (sWAT: control $n = 13$, TG $n = 10$; eWAT: control $n = 13$, TG $n = 8$). **i**, Serum adiponectin levels (control $n = 5$, TG $n = 6$). **j**, Serum leptin levels (fed: control $n = 13$, TG $n = 10$; fasted control $n = 13$, TG $n = 9$). **k**, Serum iron levels (day 2: control $n = 10$, TG $n = 9$; day 10: $n = 5$; day 12 $n = 6$; day 42: control $n = 14$, TG $n = 9$). **l**–**m**, Oral glucose tolerance test. **l**, Serum glucose levels (HFD: control $n = 22$, TG $n = 19$; HFD dox: control $n = 14$, TG $n = 11$). **m**, Serum insulin levels (HFD: control $n = 20$, TG $n = 15$; HFD dox: control $n = 11$, TG $n = 9$). **n**, Insulin tolerance test (HFD: control $n = 18$, TG $n = 13$; HFD dox: control $n = 13$, TG $n = 10$). **o**,**p**, mRNA levels of inflammation markers relative to control HFD dox in sWAT (control $n = 13$, TG $n = 7$; **o**) and eWAT (control $n = 13$, TG $n = 7$; **p**). **q**–**s**, Flow cytometric measurements in HFD dox of total macrophages (sWAT: control $n = 11$, TG $n = 16$, eWAT: control $n = 16$, TG $n = 17$; **q**), M1-like (sWAT: control $n = 18$, TG $n = 16$, eWAT: control $n = 18$, TG $n = 15$; **r**) and M2-like (sWAT: control $n = 18$, TG $n = 15$, eWAT: control $n = 17$, TG $n = 12$; **s**) macrophages in sWAT and eWAT. **t**–**w**, mRNA levels of antioxidant genes relative to control in eWAT (control $n = 13$, TG $n = 10$). Significance in **b**, **e** and **k**–**n** between control and Mac-MitoNEET^{TG} was calculated using a two-way ANOVA with Sidak's post hoc test for multiple comparisons. Significance in **c**, **d**, **g**–**j** and **o**–**w** between control and Mac-MitoNEET^{TG} was calculated using a two-tailed Student's *t*-test. Error bars represent the mean ± s.e.m. $*P < 0.05$, $**P < 0.01$, $***P < 0.001$, $****P < 0.0001$.

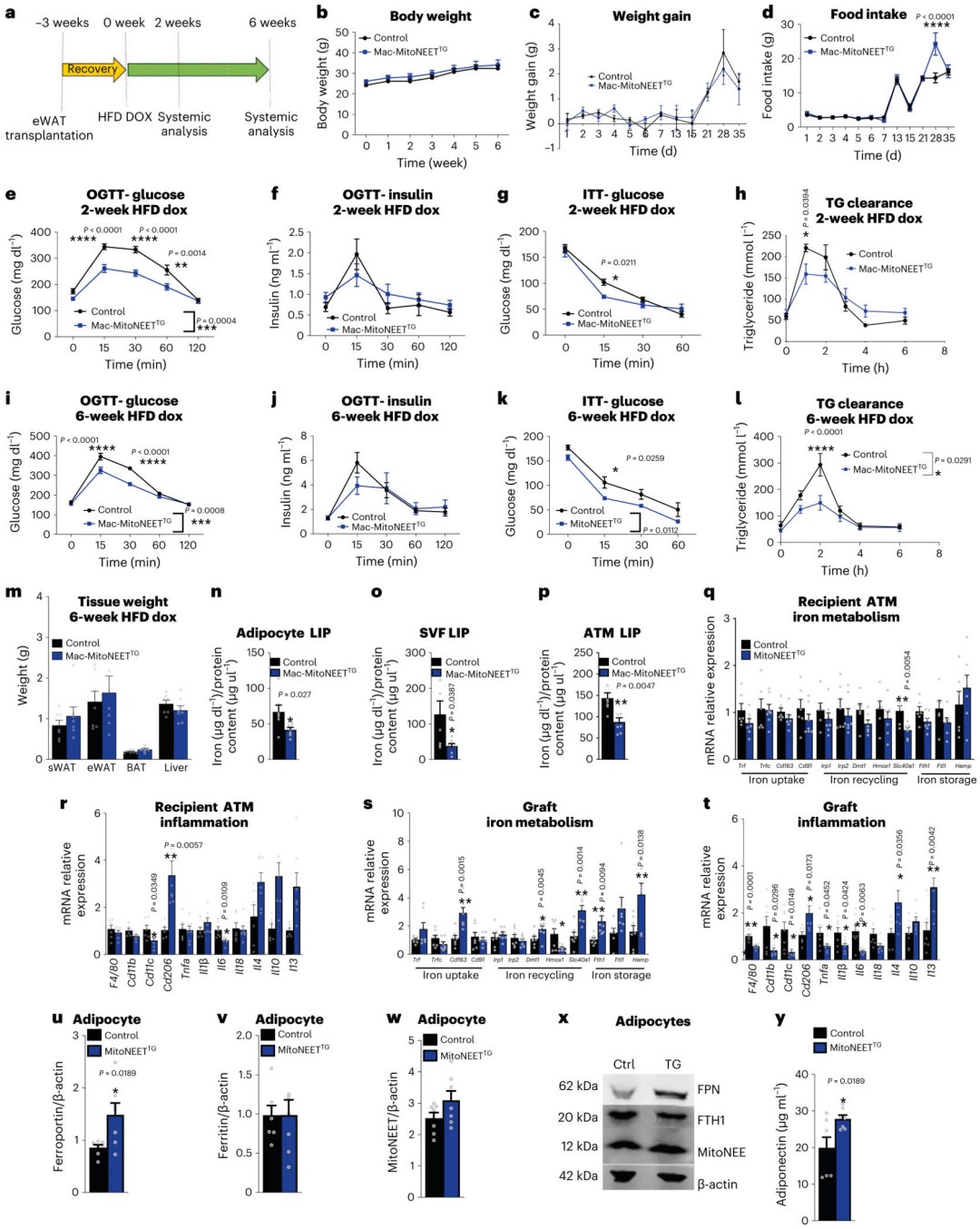

Fig. 5 |. Beneficial systemic effects in Mac-MitoNEET^{TG} mice are due to adipose tissue macrophages.

a–**y**, Six-week-old male wild-type mice were transplanted with either control or Mac-MitoNEET^{TG} eWAT and fed HFD dox for up to 6 weeks. **a**, Experimental design. **b**, Body weight ($n = 7$). **c**, Body weight gain ($n = 8$). **d**, Food intake ($n = 7$). **e**–**h**, Data after 2 weeks of HFD dox feeding. **e**,**f**, Oral glucose tolerance test ($n = 8$). **e**, Serum glucose levels ($n = 8$). **f**, Serum insulin levels ($n = 8$). **g**, Insulin tolerance test ($n = 7$). **h**, Triglyceride clearance ($n = 7$). **i**–**y**, Data after 6 weeks of HFD dox feeding ($n = 7$). **i**,**j**, Oral glucose

tolerance test ($n = 7$). **i**, Serum glucose levels ($n = 7$). **j**, Serum insulin levels ($n = 7$). **k**, Insulin tolerance test ($n = 7$). **l**, Triglyceride clearance ($n = 7$). **m**, Tissue weights ($n = 7$). **n**–**p**, Labile iron pool (LIP) in adipocytes ($n = 7$; **n**), SVF cells ($n = 7$; **o**) and ATMs ($n = 7$; **p**) from recipient eWAT. **q**,**r**, mRNA levels of iron metabolism genes (**q**) and inflammation markers (**r**) relative to control in ATMs from recipient eWAT ($n = 7$). **s**,**t**, mRNA levels of iron metabolism genes (**s**) and inflammation markers (**t**) relative to control in ATMs from grafted eWAT ($n = 7$). **u**–**w**, Ferroportin (**u**), ferritin (**v**) and MitoNEET (**w**) protein levels in adipocytes from recipient eWAT ($n = 7$). **x**, Representative western blots chosen from seven independent experiments. **y**, Serum adiponectin levels. Significance in **b**–**l** between control and Mac-MitoNEET^{TG} was calculated using a two-way ANOVA with Sidak's post hoc test for multiple comparisons. Significance in **m**–**y** between control and Mac-MitoNEET^{TG} was calculated using a two-tailed Student's *t*-test. Error bars represent the mean ± s.e.m. *$P <$ 0.05, **$P < 0.01$, ***$P < 0.001$, ****$P < 0.0001$.

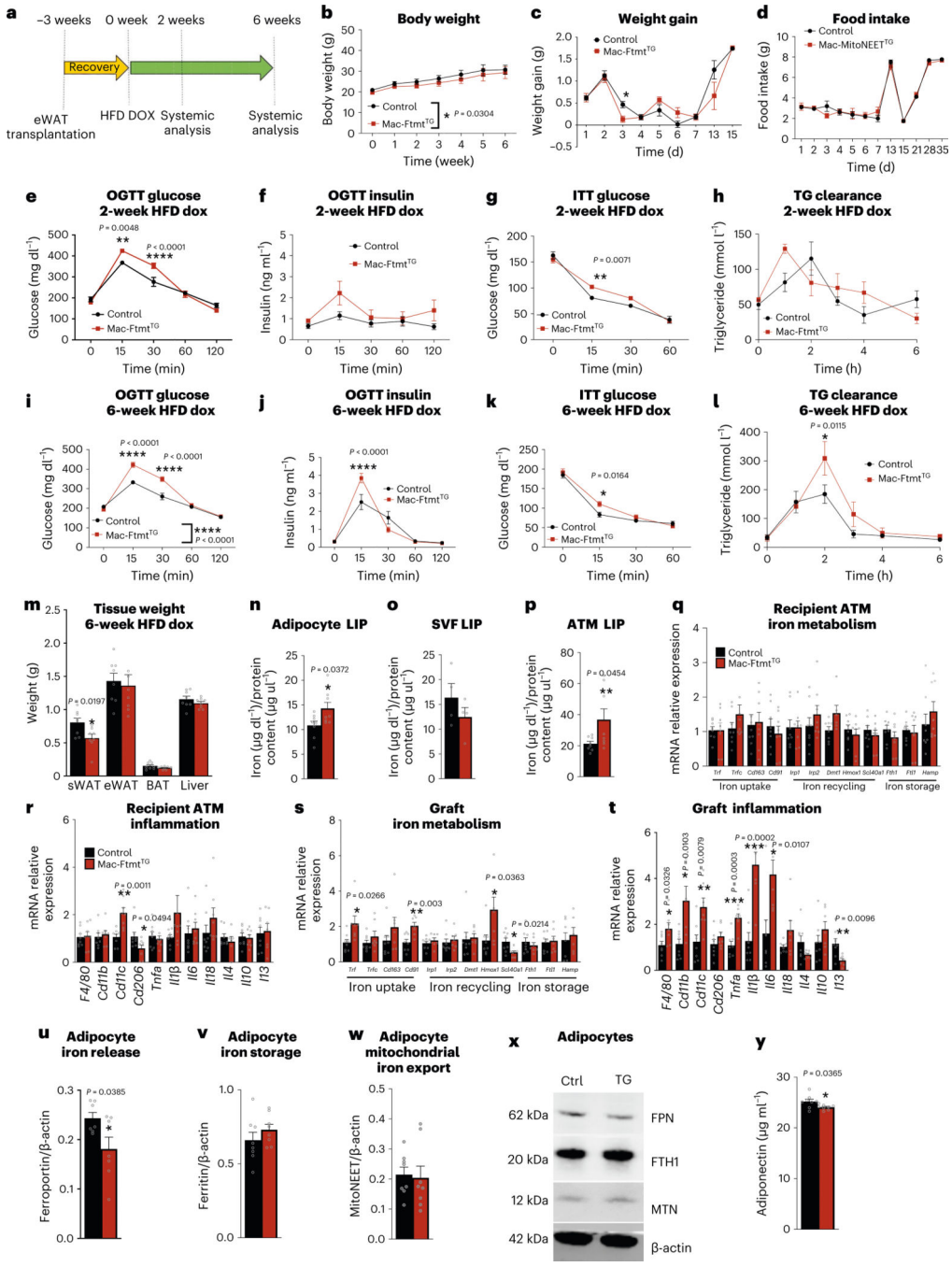

Fig. 6 |. Deleterious systemic effects in Mac-Ftmt^{TG} mice are equally due to adipose tissue macrophages.

a–**y**, Six-week-old male wild-type mice were transplanted with either control or Mac-Ftmt^{TG} eWAT and fed HFD dox for up to 6 weeks ($n = 8$). **a**, Experimental design. **b**, Body weight ($n = 8$). **c**, Body weight gain ($n = 8$). **d**, Food intake ($n = 8$). **e**–**h**, Data after 2 weeks of HFD dox feeding ($n = 8$). **e**,**f**, Oral glucose tolerance test ($n = 8$). **e**, Serum glucose levels ($n = 8$). **f**, Serum insulin levels ($n = 8$). **g**, Insulin tolerance test ($n = 8$). **h**, Triglyceride clearance ($n = 8$). **i**–**y**, Data after 6 weeks of HFD dox feeding ($n = 8$).

i,**j**, Oral glucose tolerance test ($n = 8$). **i**, Serum glucose levels ($n = 8$). **j**, Serum insulin levels ($n = 8$). **k**, Insulin tolerance test ($n = 8$). **l**, Triglyceride clearance ($n = 8$). **m**, Tissue weights ($n = 8$). **n**–**p**, Labile iron pool (LIP) in adipocytes (**n**), SVF (**o**) and ATMs (**p**) from recipient eWAT ($n = 8$). **q**,**r**, mRNA levels of iron metabolism genes (**q**) and inflammation markers (**r**) relative to control in ATMs from recipient eWAT ($n = 8$). **s**,**t**, mRNA levels of iron metabolism genes (**s**) and inflammation markers (**t**) relative to control in ATMs from grafted eWAT ($n = 8$). **u**–**w**, Ferroportin (**u**), ferritin (**v**) and MitoNEET (**w**) protein levels in adipocytes from recipient eWAT ($n = 8$). **x**, Representative western blots chosen from eight independent experiments. **y**, Serum adiponectin levels. Significance in **b**–**l** between control and Mac-Ftmt^{TG} was calculated using a two-way ANOVA with Sidak's post hoc test for multiple comparisons. Significance in **m**–**y** between control and Mac-Ftmt^{TG} was calculated using a two-tailed Student's *t*-test. Error bars represent the mean ± s.e.m. *$P < 0.05$, **$P < 0.01$, ***$P < 0.001$, ****$P < 0.0001$.

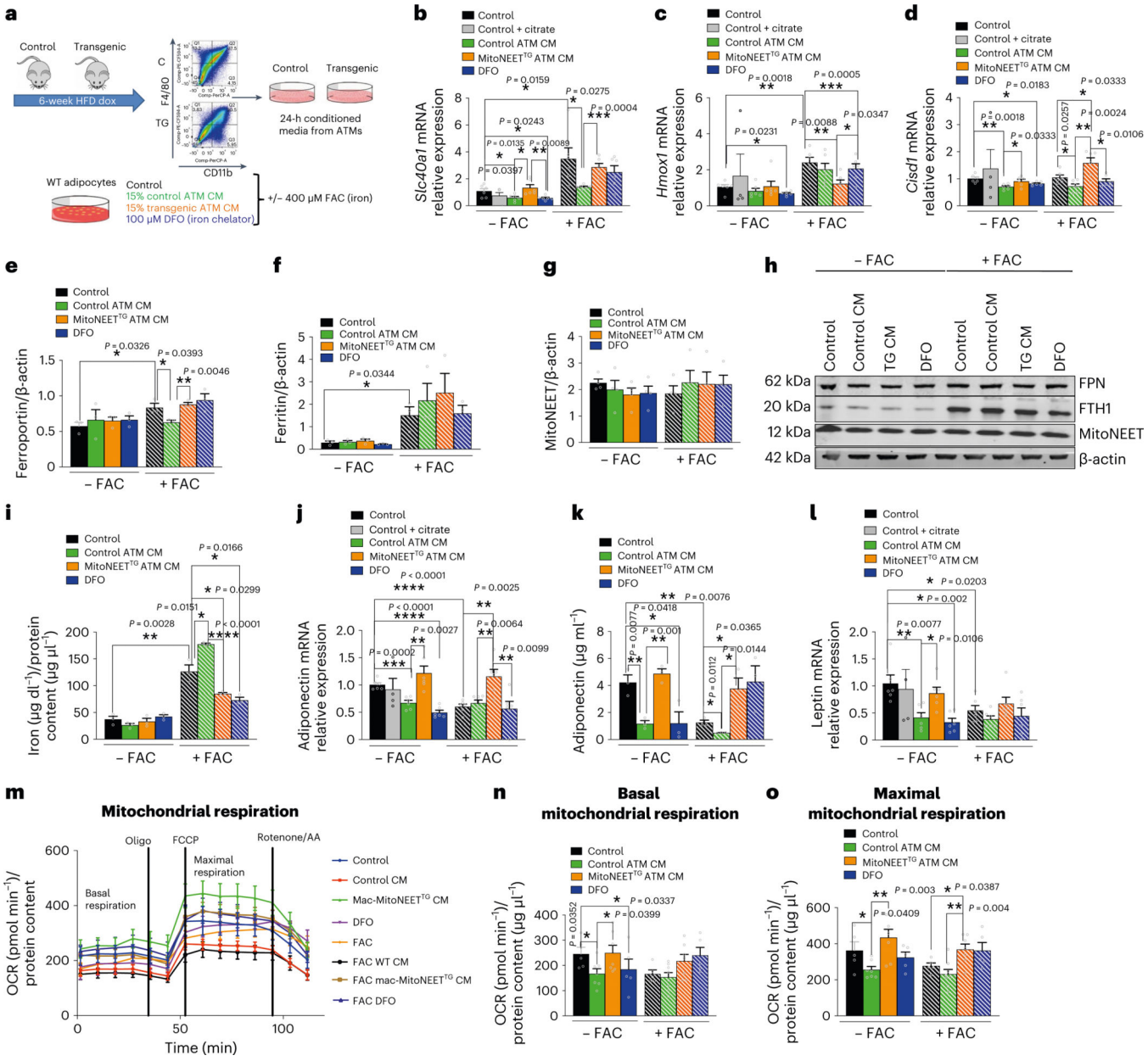

Fig. 7 |. Beneficial cross-talk between Mac-MitoNEET^{TG} ATMs and adipocytes.

a–**o**, Wild-type adipocytes were treated with 15% conditioned medium (CM) from either control or Mac-MitoNEET^{TG} ATMs (n = 6) or with 100 µM iron chelator (deferoxamine (DFO); n = 6) in the presence or absence of 400 µM of iron (FAC) or citrate (n = 4) alone for 24 h. **a**, Experimental design. **b**–**d**, *Slc40a1* (**b**), *Hmox1* (**c**) and *Cisd1* (**d**) mRNA levels relative to control (n = 6). **e**–**g**, Ferroportin (**e**), ferritin (**f**) and MitoNEET (**g**) protein levels relative to β-actin (n = 4). **h**, Representative western blots chosen from four independent experiments. **i**, Total iron content in adipocytes (n = 3). **j**, Adiponectin mRNA levels relative to control (n = 6). **k**, Supernatant adiponectin levels (n = 3). **l**, Leptin mRNA levels relative to control (n = 6). **m**–**o**, Mitochondrial respiration of adipocytes relative to protein content (n = 6). **m**, Oligomycin, carbonyl cyanide 4-(trifluoromethoxy) phenylhydrazone (FCCP)

and rotenone/antimycin were injected at 18.4, 44.7 and 95.4 min respectively. **n**, Basal mitochondrial respiration. **o**, Maximal mitochondrial respiration. Significance in **b**–**o** was calculated using a two-tailed Student's *t*-test. Error bars represent the mean ± s.e.m. *$P <$ 0.05, **$P < 0.01$, ***$P < 0.001$, ****$P < 0.0001$. OCR, oxygen consumption rate.

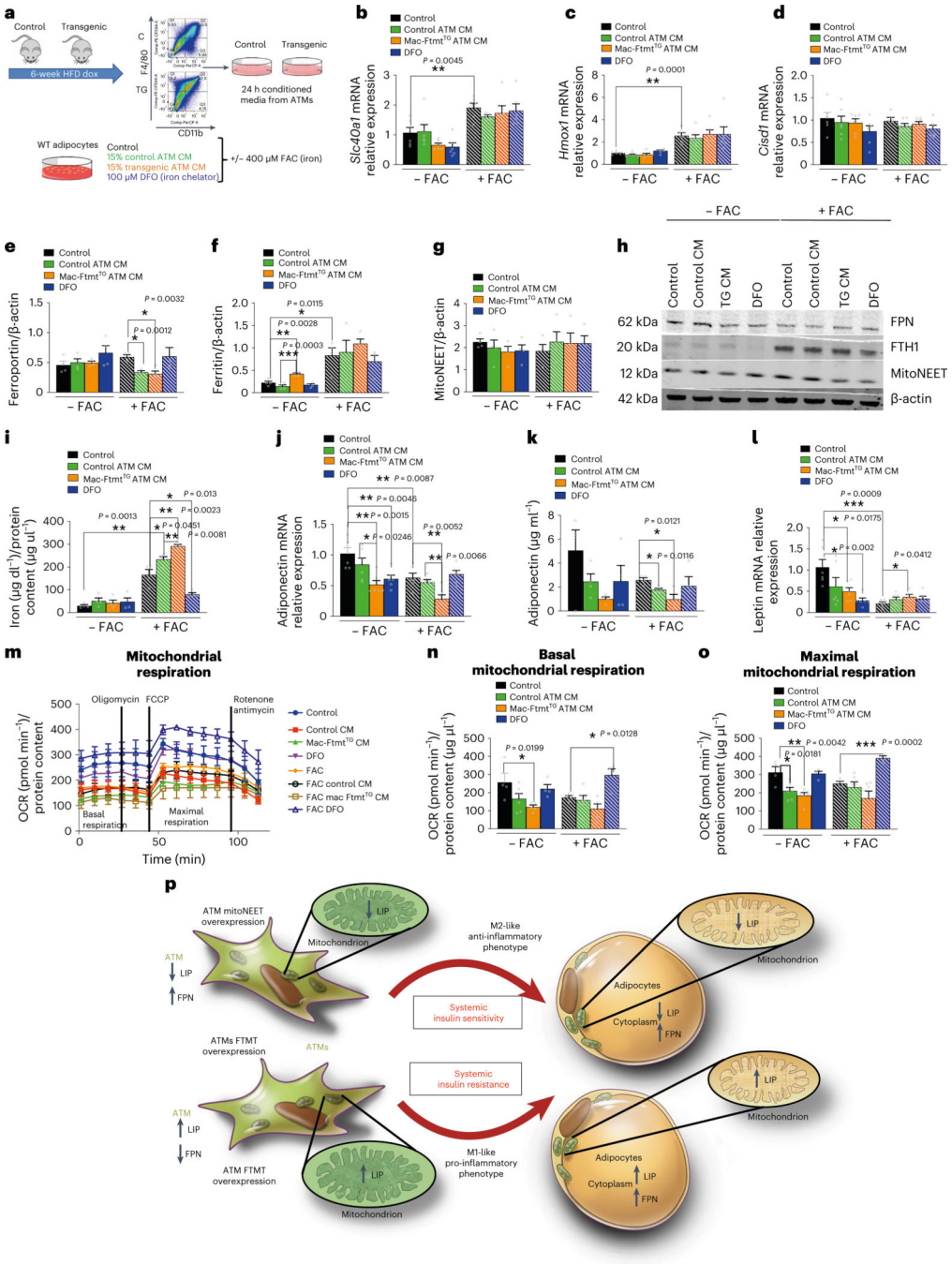

Fig. 8 |. Deleterious cross-talk between Mac-Ftmt^{TG} ATMs and adipocytes.

a–**o**, Wild-type adipocytes were treated with 15% conditioned medium from either control (n = 6) or Mac-FtmtTG ATMs (n = 6) or with 100 µM iron chelator (DFO; n = 6) in the presence or absence of 400 µM of iron (FAC) for 24 h. **a**, Experimental design. **b**–**d**, *Slc40a1*, *Hmox1* and *Cisd1* mRNA levels relative to control (n = 6). **e**–**g**, Ferroportin (**e**), ferritin (**f**) and MitoNEET (**g**) protein levels relative to β-actin (n = 4). **h**, Representative western blots chosen from four independent experiments. **i**, Total iron content in adipocytes (n = 3). **j**, Adiponectin mRNA levels relative to control (n = 6).

k, Supernatant adiponectin levels ($n = 3$). **l**, Leptin mRNA levels relative to control ($n = 6$). **m**–**o**, Mitochondrial respiration of adipocytes relative to protein content ($n = 6$). **m**, Oligomycin, FCCP and rotenone/antimycin were injected at 18.4, 44.7 and 95.4 min, respectively. **n**, Basal mitochondrial respiration. **o**, Maximal mitochondrial respiration. Significance in **b**–**o** was calculated using a two-tailed Student's *t*-test. Error bars represent the mean ± s.e.m. $*P < 0.05$, $**P < 0.01$, $***P < 0.001$, $****P < 0.0001$. **p**, A schematic for the proposed mechanism for how local labile iron concentrations (LIP) in ATMs alter adipocyte function and systemic insulin sensitivity. MitoNEET expression in ATMs lowers cellular and mitochondrial free iron levels and increases FPN, a plasma membrane iron export protein. This results in increased number of M2-like anti-inflammatory macrophages in adipose tissue. During obesity, this protects the adipocyte from iron overload, thus preserving its metabolic functions and systemic insulin sensitivity. Macrophages respond to FTMT overexpression opposite to MitoNEET overexpression, by increasing free iron levels, reducing FPN levels and stimulating a M1-like pro-inflammatory phenotype. The presence of M1-like macrophages promotes iron overload in adipocytes. Collectively, this results in exacerbated inflammation and a predisposition to systemic insulin resistance.